Catena 220 (2023) 106647

Contents lists available at ScienceDirect

Catena

journal homepage: www.elsevier.com/locate/catena

Natural revegetation over ~ 160 years alters carbon and nitrogen sequestration and stabilization in soil organic matter on the Loess Plateau of China

Wen Yang [a,*], Di Zhang [a], Xinwen Cai [a], Xitong Yang [a], Huan Zhang [a], Yaqi Wang [a], Longfei Diao [a], Yiqi Luo [b], Xiaoli Cheng [c,*]

[a] College of Life Sciences, Shaanxi Normal University, Xi'an 710119, PR China
[b] School of Integrative Plant Sciences, Cornell University, Ithaca, NY 14850, USA
[c] School of Ecology and Environmental Sciences, Yunnan University, Kunming 650091, PR China

ARTICLE INFO

Keywords:
13C and 15N
C and N stabilization
Density and size fractionation
Mineral-associated organic matter
Vegetation restoration

ABSTRACT

Natural revegetation has been reported to play a very active role in ecosystem carbon (C) and nitrogen (N) sinks in degenerated ecosystems. However, the responses of C and N sequestration and stabilization in soil organic matter (SOM) to natural revegetation remain inadequately understood. In this study, we analyzed C and N contents and $\delta^{13}C$ and $\delta^{15}N$ values of SOM, free light fraction (FLF), intra-aggregate particulate organic matter (IPOM) and mineral-associated organic matter (MAOM) along ~ 160 years of natural revegetation on the Loess Plateau of China. The results showed that natural revegetation significantly ($P < 0.05$) enhanced soil C and N contents in FLF, IPOM, MAOM, SOM in the surface soil (0–20 cm) during the later stages of revegetation, which exhibited smaller impact on the deeper soil (20–60 cm). Natural revegetation significantly increased distribution proportions of C and N in FLF (i.e., 18.00–36.00%, 8.46–22.57%, respectively), and that in IPOM (i.e., from 11.60 to 25.38%, 10.89–26.92%, respectively), while it decreased that in MAOM (i.e., from 56.25 to 37.00%, 67.69–50.24%, respectively) in the surface soil, thereby altering C and N stabilization in SOM (0–20 cm). The climax *Quercus liaotungensis* forest exhibited the highest C distribution proportion in FLF and IPOM, and the lowest C distribution proportion in MAOM in the surface soil. The $\delta^{13}C$ and $\delta^{15}N$ were enriched with the decomposition of SOM and soil profile depths at each revegetation stage. The highest $\delta^{13}C$ and $\delta^{15}N$ values (0–60 cm) and the lowest C:N ratio (0–20 cm) of SOM, FLF, and IPOM were found in the farmland. In conclusion, ~160 years of natural revegetation substantially promoted C and N sequestration in SOM, whereas altered C and N stabilization in SOM of the surface soil through shifting C and N towards more non-protected and pure physically protected SOM fractions rather than the most stable MAOM. Meanwhile, soil $\delta^{13}C$ and $\delta^{15}N$ in SOM and its fraction were changed along with natural revegetation. The most enriched soil $\delta^{15}N$ in the farmland implied that soil N cycle in the farmland was more open to N losses relative to the other revegetation stages.

1. Introduction

Unreasonable land use, particularly in the forms of excessive logging and the transition of ambient forests to farmland, is a global issue that has led to the loss of natural vegetation, land degradation, and seriously threaten forest ecosystem services (Khormali et al., 2009; Karchegani, et al., 2011; Zhang et al., 2020; Ayoubi et al., 2021). Currently, forest restoration is a global priority (Suding et al., 2015; Crouzeilles et al., 2016) as two billion hectares of forests have been degraded worldwide and identified as requiring either passive (i.e., natural revegetation) or active (i.e., afforestation) forest restoration (Minnemeyer et al., 2011; Crouzeilles et al., 2016). Natural revegetation has been widely confirmed to be a viable approach for the revitalization of damaged ecosystems through the renewal of supportive environments, facilitating soil and water preservation (Sun et al., 2015), to augment the efficiency of ecosystems (Ayoubi et al., 2011; Baker and Eckerberg, 2016). Under natural revegetation the functional traits of plants (Wang et al., 2022), as well as the composition, structure, coverage, and biodiversity of

* Corresponding authors at: College of Life Sciences, Shaanxi Normal University, No. 620 West Chang'an St., Chang'an Dist., Xi'an 710119, PR China (W. Yang).
E-mail addresses: wenyang@snnu.edu.cn (W. Yang), xlcheng@fudan.edu.cn (X. Cheng).

https://doi.org/10.1016/j.catena.2022.106647
Received 24 March 2022; Received in revised form 30 August 2022; Accepted 14 September 2022
Available online 29 September 2022

vegetation communities were observed to be greatly altered (Crouzeilles et al., 2016; Krishna et al., 2020). These adjustments alter amounts and qualities of plant residue inputs into soil, the physicochemical attributes of soil (Rosenzweig et al., 2016), soil water patterns (Chen et al., 2022), and soil microbe populations (Krishna et al., 2020; Cai et al., 2022). Ultimately, these factors can dramatically impact the cycles of carbon (C) and nitrogen (N) in ecosystems (Sullivan et al., 2019), particularly in terms of soil C and N sequestration (Yang et al., 2019; Lv et al., 2021; Wang et al., 2021; Wang et al., 2022).

Natural revegetation has been identified as a promising avenue for the mitigation of climate change by facilitating C and N sequestration in both plants and soil (Deng et al., 2014; Hancock et al., 2019). Globally, the average cumulative rates for soil organic carbon (SOC) and total nitrogen (TN) were 33.8 g C m^{-2} $year^{-1}$ and 0.9 g N m^{-2} $year^{-1}$, respectively, for forests that emerged on former agricultural lands (Zhong et al., 2021). Although the impacts of natural revegetation on soil C and N sequestration are widely documented (Deng et al., 2013; Gao et al., 2020; Khorchani et al., 2022), these studies primarily set their focus on variations in the total SOC and TN concentrations, or stocks (Deng et al., 2013; Gao et al., 2020). While, it remains inadequately understood exactly how C and N in soil organic matter (SOM) are stabilized through natural revegetation. Stabilization refers to a decrease in the potential loss of C and N in SOM (Pinheiro et al., 2015). The C and N in SOM are stabilized through three primary mechanisms: (i) physical protection by soil aggregates; (ii) chemical association among C and fine soil particles (e.g., clay, silt, Fe and Al oxides); (iii) biochemical recalcitrance of soil organic molecules (Sollins et al., 1996; Briedis et al., 2018). Physicochemical stabilization of C and N in SOM, and composition of organic matter (OM) play crucial roles in deciding the persistence of C and N in terrestrial ecosystems (Williams et al., 2018). Thus, elucidating how natural revegetation impacts the C and N sequestration and stabilization in SOM is essential for estimating the long-term acquisition and storage of soil C and N, and their influences on climate change.

The constituents of SOM encompass a highly diverse array of organic components of different origins (Prater et al., 2020), which may be partitioned into separate operational fractions with varying microbial accessibility (Startsev et al., 2020), turnover times (Yeasmin et al., 2020), and stabilizing strategies (Samson et al., 2020). Soil physical fractionation based on density and particle size has been broadly utilized to divide raw SOM samples into three distinct segments (Six et al., 1998; Pinheiro et al., 2015). These include a free light fraction (FLF) and intra-aggregate particulate organic matter (IPOM), which are mainly comprised of new and partly decayed plant residues (Christensen, 1992; Samson et al., 2020; Francisco et al., 2021). The FLF is not protected through physical or chemical means by soil, and exhibits rapid decomposition rates and turnover times, which is recognized as an active soil pool (Wander, 2004; Yang et al., 2017; Williams et al., 2018). IPOM represents a slowly mineralized soil pool with a longer turnover time relative to FLF, owing to its being physically protected by soil aggregates (Six et al., 1998; Wander, 2004; Marín-Spiotta et al., 2008; Kauer et al., 2021). The third fraction is mineral-associated organic matter (MAOM), which is considered to be a passive soil pool with the lowest bioavailability and decomposition rate, and the longest residence time in soil across SOM fractions via chemical bonding to silt- and clay-sized mineral particles (Karchegani et al., 2012; Lavallee et al., 2020; Macedo et al., 2021; Pierson et al., 2021). Therefore, a comprehensive assessment of the impacts of natural revegetation on C and N allocations in SOM, FLF, IPOM, and MAOM have significant implications toward elucidating stabilizing kinetics of soil C and N as impacted by natural revegetation.

The combination of stable C and N isotopic signatures and soil physical fractionation methods can provide effective data for investigating SOM formation and persistence (Santos et al., 2020), and C and N pathways within and between SOM fractions (Atere et al., 2020). The different photosynthetic pathways of C_3 and C_4 plants leads to fixing of biomass C with distinct isotopic indicators, which assists with tracking alterations in SOC pool (Santos et al., 2020; Minick et al., 2021). Distinct $\delta^{13}C$ that is naturally presented by C_3 (mean $\delta^{13}C \approx -28‰$) and C_4 plants (mean $\delta^{13}C \approx -12‰$) allows for the identification of dynamic modifications in OM as freshly obtained plant C materials are integrated into existing OM in soils (Skjemstad et al., 1990; Minick et al., 2021). Soil $\delta^{15}N$ may be employed as a reliable tracer to reveal N cycling (Feyissa et al., 2020), where its value of SOM fractions may be combined with soil N cycling processes to assess the level of SOM decomposition and conversion of microbes (Yang et al., 2017). Generally, enriched soil $\delta^{15}N$ values represent a greater level of SOM decomposition (Plaza et al., 2016; Prater et al., 2020), which is the result of microbes preferentially metabolizing ^{14}N, and due to the integration of microbe compounds; thus, enhancing $\delta^{15}N$ with SOM decomposition (Kramer et al., 2017; Minick et al., 2021). Consequently, accurate assessment of variations in $\delta^{13}C$ and $\delta^{15}N$ values of SOM fractions along with natural revegetation can better elucidate the dynamic shifts in soil C and N cycling processes during natural revegetation.

The Loess Plateau, which inhabits the mid and upper ranges of the Yellow River in China, spans 624,000 km^2 (Zhong et al., 2021). It is one of the world's most highly vulnerable and extremely eroded regions (Fu et al., 2011). Toward the resolution of these environmental challenges since the 1950′s, significant interventions have been undertaken by the government of China (Zhong et al., 2021). The most important endeavor was the introduction of the largest ecological engineering "Grain for Green" program in China in 1999, which involved the conversion of croplands at inclines of>15° to grassland, shrubland, or forest through natural revegetation or afforestation (Deng et al., 2014). To date, this project has transformed > 16,000 km^2 of farmland on the Loess Plateau to grassland or forest (Xu et al., 2018), leading to a 28% increase in vegetation cover from 1999 to 2013, and a 87.5% decrease in sediments flowing into the Yellow River. Earlier research has recorded the variations in soil C and N concentrations or stocks to the active renewal of vegetation (i.e., afforestation) (Han et al., 2019; Song et al., 2021), or short-term natural revegetation (<50 years) (Deng et al., 2016) in this region. However, the effects of protracted (>150 years) natural revegetation on the reserves and stabilization of C and N in SOM pool remain unknown. In current study, we hypothesize that: (i) long-term natural revegetation increases C and N sequestration in SOM and its fraction, and the climax forest possesses the greatest C and N sequestration in SOM and its fraction; (ii) long-term natural revegetation alters the C and N stabilization in SOM through shifting C and N towards more non-protected and pure physically protected SOM fractions, and correspondingly reducing C and N allocations in the most stable MAOM; (iii) The $\delta^{13}C$ and $\delta^{15}N$ values in SOM and its fraction were modified along with long-term natural revegetation. The farmland possesses the most enriched $\delta^{13}C$ and $\delta^{15}N$ values in SOM. To test this hypothesis, we coupled soil physical fractionation procedures and the analysis of stable isotopes to analyze organic C and TN concentrations and stocks, C:N ratio, and $\delta^{13}C$ and $\delta^{15}N$ values in SOM, FLF, IPOM, and MAOM. Furthermore, we examined the concentrations of soil microbial biomass C and N (MBC and MBN, respectively), and soil physiochemical attributes, i.e., soil pH, moisture, and bulk density (BD), and plant characteristics (i.e., litter/root biomass, litter C:N ratio) at several soil depths (0–20, 20–40, and 40–60 cm) along with ~ 160 years natural revegetation of former farmland to stages of pioneer weed, herb, shrub, to early forest, and eventually to climax forest.

2. Materials and methods

2.1. Study site

This investigation was conducted in the Ziwuling Mountains (northwest face), in the central Loess Plateau region (36°00′14″–36°01′09″N and 109°00′56″–109°01′52″E), in Fu County, Shaanxi Province, China (Fig. 1a and b). This area is characterized by

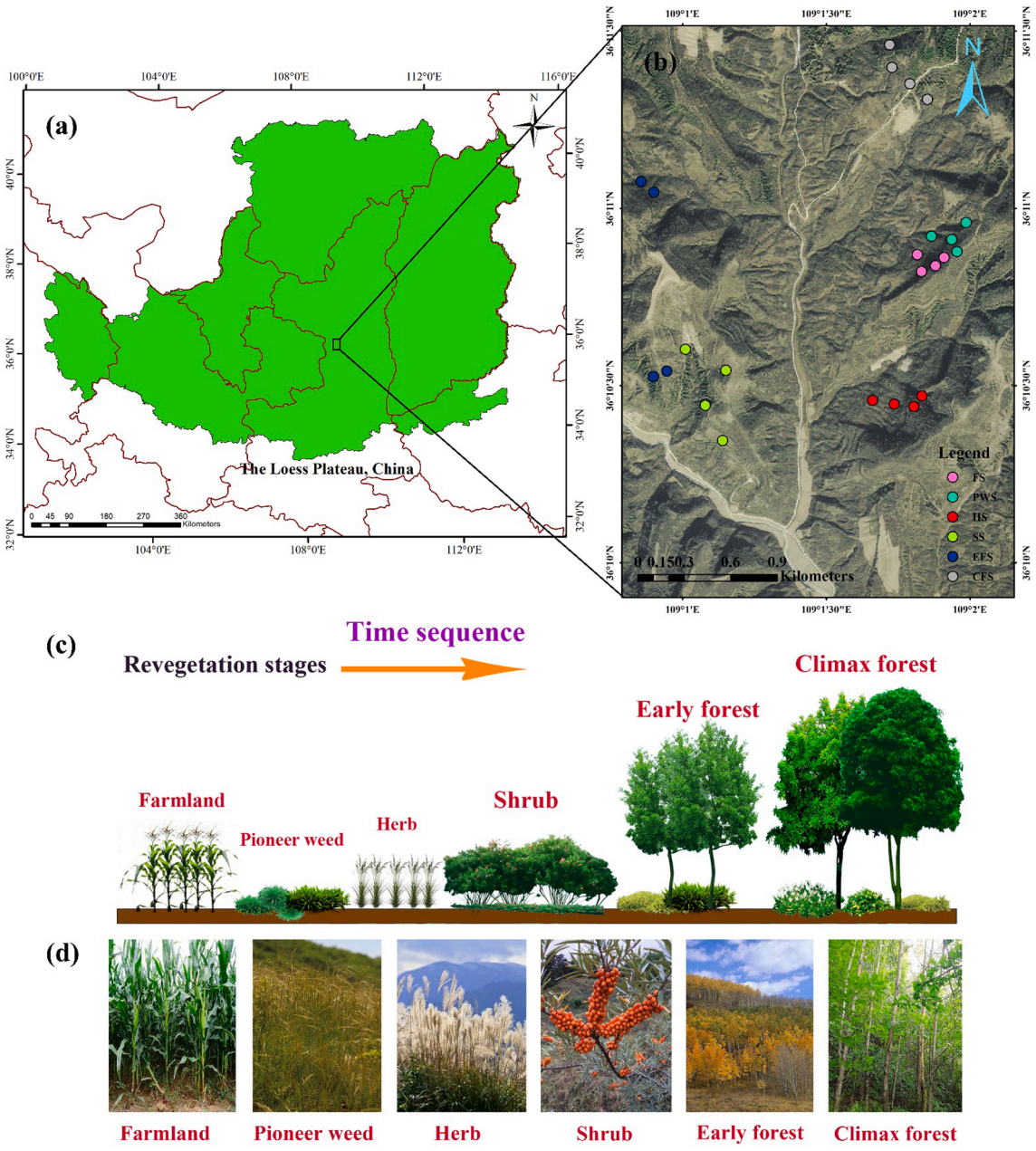

Fig. 1. (a) Geographic coordinates of Loess Plateau of China, (b) Locations of the sampling sites in the in Fu County, Shaanxi Province, China. Pink circles represent sampling plots of farmland stage (FS); sky blue circles represent sampling plots of pioneer weed stage (PWS); red circles represent sampling plots of herb stage (HS); yellow circles represent sampling plots of shrub stage (SS); dark blue circles represent sampling plots of early forest stage (EFS); grey circles represent sampling plots of climax forest stage (CFS), (c) conceptual diagram of primary stages during natural revegetation process, (d) photographs of study location for each revegetation stage. (For interpretation of the references to colour in this figure legend, the reader is referred to the web version of this article.)

typical hilly and gullied landscapes with altitudes that range from 1157 to 1369 m asl (above sea level) (Yan et al., 2020). The continental monsoon climate of this region has an average yearly temperature and rainfall of 9 °C and 576.7 mm, respectively. The soil is of the cinnamon type and categorized as Ustalfs according to the USDA Soil Taxonomy. This area has undergone intense soil erosion due to its loose soil and incessant human interference. The combination of natural revegetation with continued deforestation in the Ziwuling Mountain region has induced the emergence of secondary forests that span ~ 23,000 km^2.

In the study area natural revegetation revitalized deserted agricultural lands, where *Zea mays L.* was the original main crop (Zhong et al., 2018). Since 1860, the abandonment of this land occurred a number of times when the local population was displaced due to war, food scarcity, and other disasters. As a consequence, over the last ~ 160 years various revegetation stages have been observed, ranging from pioneer weeds, to herbs, to shrubs, to early and climax forests (Zhong et al., 2018). Chen et al. (1954) revealed that *Populus davidiana* Dode was the dominant species in this region following ~ 100 years of revegetation. The ages of pioneer weeds, herbs, and shrubs was determined through discussions with local elders, and by investigating land agreements between farmers and the government. Six typical natural revegetation stages were selected as samples for this investigation: (1) farmland stage (control, 0-yr., FS) where *Zea mays L.* was the primary rotation crop before revegetation; (2) pioneer weed stage (~15 yrs., PWS) dominated by *Artemisia lavandulaefolia* DC and *Stipa bungeana* Trin.; (3) herb stage (~30 yrs., HS) where *Triarrhena sacchariflora* (Maxim.) Nakai was the primary dominant species; (4) shrub stage (~50 yrs., SS), *Hippophae rhamnoides Linn.* community was predominant; (5) early forest stage (~110 yrs.,

EFS) dominated by *P. davidiana*; and (6) climax forest stage (~160 yrs., CFS) dominated by *Quercus liaotungensis* Koidz (Fig. 1c, d). The geographical data and vegetation characteristics for each revegetation stage in this study are shown in Table S1.

2.2. Field sampling

Samples were gathered in October 2019, and four replicate plots were randomly established for each revegetation stage (Fig. 1b). The plot sizes were 2 m × 2 m for the farmland, pioneer weed, and herb communities, 5 m × 5 m for the shrub community, and 20 m × 20 m for the early and climax forests, respectively. To reduce the impacts of the localized site environments on the results, the distances between adjacent plots for each revegetation stage were 100 m at minimum, but not greater than 2 km at elevations lower than 120 m. All surveyed soils were developed from the same parent materials (i.e., loess parent material) and soil type (i.e., cinnamon soil). For each revegetation phase, all plots were on similar slope gradients and aspects to ensure equivalent environments. The S-shaped sampling technique was employed to randomly extract nine soil samples (5 cm diameter × 20 cm deep) from each plot at 0–20, 20–40, and 40–60 cm depths, respectively. The soil samples from each layer of every plot were completely mixed to produce a single composite. Overall, 72 soil cores were obtained (24 plots × 3 soil depths). A cutting ring was employed for the 0–20, 20–40, and 40–60 cm soil depths to ascertain the bulk soil density for each plot. Three 1 × 1 m quadrats from each plot were selected at random for litter sample collection. A total of three root sample cores (10 cm diameter × 20 cm deep) from each plot were stochastically extracted with a root drill at soil depths of from 0 to 20, 20–40, and 40–60 cm, respectively. Thus, 72 litter and 216 root samples were obtained.

2.3. Laboratory analyses

The soil samples were cleared of all roots and organic debris, followed by sifting through a 2 mm sieve and complete mixing, after which they were segregated as three subsamples. To quantify the soil moisture, the first subsample was dried at 105 °C to a constant weight, whereas to assess soil pH the second subsample was dried in ambient air and passed through a 1 mm sieve. The third subsample was dried in ambient air and sifted through a 2 mm sieve to determine the C and N concentrations in the SOM, FLF, and IPOM. The fresh soil and solid soil cores that were extracted with the cutting ring were heated to 105 °C and dried to an even weight to quantify the soil moisture and bulk density, respectively. The soil pH was determined with a pH meter, and the soil/water ratio was 1:2.5. The microbial biomass C (MBC) and microbial biomass N (MBN) concentrations were quantified using the chloroform fumigation-extraction technique (Vance et al., 1987). Each root sample block was continuously rinsed with water using a 0.15 mm sieve, after which the remaining roots were collected. Subsequently, the litter and root samples were thoroughly cleaned and dried in an oven at 65 °C to a constant weight to measure the biomass of litter and roots, respectively.

2.4. Physical fractionation of SOM

To achieve functionally distinct SOM pools, the soil samples were separated via combined density and size fractionation using a technique derived from Six et al. (1998), Yang et al. (2017), and Samson et al. (2020). To summarize, a 25 g of 2 mm air-dried sample was placed in a 100 mL centrifuging tube with 50 mL of a 1.70 g cm^{-3} NaI solution. The tube was then stoppered and shaken for 1 h at 200 rpm, and the soil suspension was centrifugated at 1000 × g for 20 min. The FLF that floated on the NaI supernatant was separated with a 0.45 μm nylon membrane using a glass vacuum filtration device. The material that lingered on the filter was then cleaned using 75 mL of 0.01 M $CaCl_2$ to remove any residual NaI, which was followed by 100 mL of ultrapure water. The materials that floated within the centrifuge tube were extracted twice with NaI, and these two subfractions were transferred to a pre-weighed 50 mL glass beaker using ultrapure water, heated and dried at 50 °C and weighed to create a FLF sample (Yang et al., 2017; Samson et al., 2020). The soil remaining at the bottom of the centrifuge bottle was rinsed twice with 50 mL of ultrapure water, centrifuged, and the supernatant was removed. The washed soil sample was dispersed in 0.5% sodium hexametaphosphate (SHMP), and soil suspension was sifted through a 53 μm sieve to separate IPOM from MAOM, and the detailed separation method of IPOM and MAOM was in line with Six et al. (1998), and our previously described methods (Yang et al., 2017). The obtained IPOM and MAOM samples were dried in an oven at 50 °C and weighed.

2.5. C and N concentrations and stable isotope measurements

To eliminate the total inorganic C, the bulk soil (i.e., whole SOM), FLF, IPOM, and MAOM fractions acquired through the soil fractionation process were subjected to 1 M HCl at room temperature for 24 h. The oven-dried SOM fractions were pulverized in a ball mill to prepare them for organic C and TN concentration, and isotope analyses for C and N. The concentrations of C and N in the SOM fractions and plant materials were measured using a Vario PYRO cube elemental analyzer (Elementar Analysensystem, Germany). On average, after using this fractionation procedure, the soil mass recovery was 94.1%, C recovery was 93.9%, and N recovery was 93.5%. The stable C and N isotopes of the SOM fractions were evaluated using an IsoPrime100 isotope ratio mass spectrometer (Isoprime Ltd., Cheadle Hulme, UK). The ratios of the stable C and N isotopes were conveyed in δX (‰) as follows:

$$\delta X = [(R_{SAMPLE}/R_{STANDARD}) - 1] \times 1000‰ \quad (1)$$

Where X is C or N, R_{SAMPLE} is the ($^{13}C/^{12}C$) or ($^{15}N/^{14}N$) ratio, and $R_{STANDARD}$ is the Pee Dee Belemnite standard $^{13}C/^{12}C$ ratio, or the $^{15}N/^{14}N$ ratio of the atmospheric N_2. Following every twelfth sample, standards were determined, and the precision of the recurrent measurements was ± 0.15‰ for $\delta^{13}C$ and ± 0.2‰ for $\delta^{15}N$, respectively.

Soil C or N stock (g m^{-2}) of each SOM fraction were determined using the equation below:

$$\text{Soil C or N stock} = \text{Con.} \times \text{BD} \times \text{T} \times 10 \quad (2)$$

where Con. is the concentration of organic C or TN for each SOM fraction (g kg^{-1}), BD is the density of the bulk soil (g cm^{-3}), and T is the soil layer thickness (cm).

2.6. Statistical analyses

The analysis of all data was performed with SPSS 24 statistical software. The data were tested for normalcy and variance homogeneity, and the data with non-normal distribution and/or non-variance homogeneous were log- or cube root-converted to satisfy suppositions for statistical analysis. One-way ANOVA was used to assess the influences of both natural revegetation and soil depth on the root biomass, soil pH, moisture, BD, MBC, MBN, C and N concentrations, SOM fraction stocks, $\delta^{13}C$ and $\delta^{15}N$ values of SOM fractions, C and N distribution proportions in SOM fractions, and C:N ratios of SOM fractions, respectively. The impacts of natural revegetation on the biomass, content of C and N, and litter C:N ratios were determined by One-way ANOVA. Significant variations between the means of the groups were evaluated with Duncan's test at $P < 0.05$. Two-way ANOVA was used to determine the effects of natural revegetation, soil depth, and their interactions on plant and soil attributes, C and N concentrations, $\delta^{13}C$ and $\delta^{15}N$, and C:N ratios of SOM fractions. Pearson's correlation analysis was performed to examine the association between C and N in SOM fractions and plant soil properties.

3. Results

3.1. Characteristics of plants and soil

Within the 0–20 cm soil layer, root biomass was greatest in the farmland, early forest, and climax forest between revegetation stages (Table S2). However, root biomass of the 20–60 cm soil layers exhibited no significant changes between revegetation stages (Table S2). Litter biomass progressively increased along with natural revegetation and attained its maximum in the climax forest (Fig. S1a). The litter C:N ratio was greatest in the climax forest and least in the farmland between revegetation stages (Fig. S1b). Natural revegetation substantially impacted on root biomass, soil pH, moisture, MBC, and MBN (Table 1). The pH of the 0–20 cm soil layer gradually declined along with natural revegetation (Table S2). Soil moisture (0–20 cm) was greatest in the climax forest, being followed by early forest, shrub, and pioneer weed, and lowest in the herb and farmland stages (Table S2). Soil BD (0–20 cm) was greatest in the farmland and herbs between revegetation stages (Table S2). The concentrations of MBC and MBN (0–20 cm) progressively increased along with natural revegetation (Table S2). Soil moisture (20–40 cm), as well as BD, MBC, and MBN (20–60 cm) showed negligible changes along with natural revegetation (Table S2). Soil pH, moisture, BD, MBC, and MBN were substantially impacted by soil depth (Table 1). Soil MBC and MBN concentrations declined in step with deeper soil layers for each revegetation stage (Table S2).

3.2. C and N concentrations and stocks of SOM fractions

Natural revegetation significantly ($P < 0.001$) impacted on organic C and total N in SOM, FLF, and IPOM, while it had no significant influence ($P > 0.05$) on organic C and total N in MAOM (Table 1). The organic C concentration and stock of SOM, FLF, and IPOM in the 0–20 cm soil layer for both climax forest and early forest were considerably greater than those of shrub, herb, pioneer weed, and farmland (Table 2, Fig. 2a, b, d). The organic C stock of MAOM in the 0–20 cm soil layer was greatest in the climax forest and smallest in the herb stage between revegetation stages (Fig. 2c). The organic C concentration and stock of SOM (20–40 cm), FLF and IPOM (20–60 cm) were greatest in the climax forest between revegetation stages (Table 2, Fig. 2a, b, d). The organic C stock of SOM in the 40–60 cm soil layer, and MAOM in the 20–60 cm soil layers were not statistically significant between revegetation stages (Fig. 2c). The total N concentration and stock of SOM, as well as the N stock of FLF (0–20 cm) in the climax forest and early forest were substantially higher in contrast to the other revegetation stages (Table 2, Fig. 2e, h). The total N concentration and stock of IPOM (0–20 cm) in the herb and farmland stages were markedly lower than those in the other revegetation stages (Table 2, Fig. 2f). The total N concentration and stock of MAOM in the 0–20 cm soil layer were highest in the climax forest and lowest in the shrub stage (Table 2, Fig. 2g). The total N stock of FLF in the 20–40 cm soil layer, and IPOM in the 20–60 cm soil layer were highest in the climax forest between revegetation stages (Fig. 2e, f). The total N stock of SOM (20–40 cm), total N concentration of MAOM (20–40 cm), and total N concentration and stock of SOM and MAOM in the 40–60 cm soil layer changed little between revegetation stages (Table 2, Fig. 2g, h). The organic C and total N concentrations in SOM, FLF, IPOM, MAOM were strongly impacted by the soil depth (Table 1). The organic C and total N concentrations and stocks of SOM, FLF, IPOM, and MAOM in the 0–20 cm soil layer were considerably greater than those in the 20–40 and 40–60 cm soil layers for each revegetation stage, except for the C concentration and stock of IPOM in the farmland, and organic C and total N stocks of MAOM for the shrub (Table 2, Fig. 2). The organic C and total N concentrations and stocks of SOM, FLF, IPOM, and MAOM for each revegetation stage revealed no significant difference between the soil layers of 20–40 and 40–60 cm, with very few exceptions (Table 2, Fig. 2). The C:N ratios of SOM and IPOM in the 0–20 cm soil layer, and of SOM and FLF in the 20–60 cm soil layer progressively increased along with natural revegetation (Fig. 3). The C:N ratio of IPOM in the 20–60 cm soil layer, and of MAOM in the 20–40 cm soil layer were highest in the farmland (Fig. 3b, c). The C:N ratio of MAOM in the 0–20 cm and 40–60 cm soil layers remained virtually unchanged, respectively, under natural revegetation (Fig. 3a, c). The C:N ratio of FLF in the 0–60 cm soil layers was markedly higher than that of SOM, IPOM, and MAOM for each revegetation stage (Fig. 3).

3.3. C and N distribution in SOM fractions

The FLF in the 0–60 cm soil layers accounted for 0.49–3.58% of the bulk weight of the soil (Fig. 4); however, it comprised 7.75–36.00% of the organic C in SOM (SOM-C) content, and 2.76–22.57% of the total N in SOM (SOM-N) content across revegetation stages (Fig. 5a and d). The IPOM in the 0–60 cm soil layers made up 10.46–23.31% of the bulk weight of the soil (Fig. 4), which comprised 9.11–25.38% of the SOM-C content and 5.78–32.18% of the SOM-N content across revegetation stages (Fig. 5b and e). The MAOM within the 0–60 cm soil layers made

Table 1
Statistical significance (F value $^{P\ value}$) of the impacts of revegetation stage, soil depth, and their interactivity on plant and soil attributes and C and N in SOM fractions (0–60 cm) based on two-way ANOVA.

Source of variation	RB	pH	Moisture	BD	MBC	MBN	SOM-C	FLF-C	IPOM-C
Revegetation stage	9.111***	16.711***	7.031***	1.209	76.413***	19.941***	29.501***	41.593***	30.918***
Soil depth	76.636***	113.704***	12.148***	3.944*	1769.527***	703.404***	441.649***	232.186***	211.223***
Revegetation stage × Soil depth	4.710***	2.529*	5.276***	0.761	60.954***	13.283***	19.309***	17.360***	15.653***
Source of variation	MAOM-C	SOM-N	FLF-N	IPOM-N	MAOM-N	δ^{13}C-SOM	δ^{13}C-FLF	δ^{13}C-IPOM	δ^{13}C- MAOM
Revegetation stage	1.590	7.919***	32.949***	17.373***	1.801	49.178***	114.596***	64.033***	6.284***
Soil depth	75.535***	256.247***	402.298***	147.331***	81.244***	30.831***	56.945***	42.068***	20.332***
Revegetation stage × Soil depth	2.320	7.187***	23.479***	6.726***	3.250**	0.521	1.043	0.899	0.359
Source of variation	δ^{15}N-SOM	δ^{15}N-FLF	δ^{15}N-IPOM	δ^{15}N-MAOM	C:N ratio-SOM	C:N ratio-FLF	C:N ratio-IPOM	C:N ratio-MAOM	
Revegetation stage	9.336***	92.703***	41.728***	38.277***	12.024***	13.777***	3.162*	1.300	
Soil depth	280.862***	832.544***	583.712***	481.291***	75.534***	9.757***	5.011*	28.373***	
Revegetation stage × Soil depth	1.658	4.382***	3.474**	2.463*	3.259**	3.463**	4.405***	1.255	

RB: root biomass; BD: bulk density; SOM: soil organic matter; free LF: free light fraction; iPOM: intra-aggregate particle organic matter; mSOM: mineral-associated SOM; SOM-C: organic carbon concentration in SOM; free LF-C: organic carbon concentration in free LF; iPOM-C: organic carbon concentration in iPOM; mSOM-C: organic carbon concentration in mSOM; SOM-N: total nitrogen concentration in SOM; free LF-N: total nitrogen concentration in free LF; iPOM-N: total nitrogen concentration in iPOM; mSOM-N: total nitrogen concentration in mSOM. δ^{13}C: the δ^{13}C value; δ^{15}N: the δ^{15}N value; C:N ratio: the carbon:nitrogen ratio.

* $P < 0.05$;

** $P < 0.01$;

*** $P < 0.001$.

Table 2
Concentrations of organic C and total N (mean ± SE, n = 4) in SOM fractions during various revegetation stages on the Loess Plateau of China.

Revegetation stages	Soil depth (cm)	C (g C kg^{-1})				N (g N kg^{-1})			
		SOM	FLF	IPOM	MAOM	SOM	FLF	IPOM	MAOM
Farmland	0–20	9.74 ± 0.64^{CDa}	2.27 ± 0.12^{CDa}	1.10 ± 0.25 ^{Da}	5.53 ± 0.68^{ABa}	1.175 ± 0.055^{BCa}	0.148 ± 0.003^{CDa}	0.127 ± 0.014^{Ba}	0.797 ± 0.049^{BCa}
(FS)	20–40	5.16 ± 0.47^{ABb}	0.49 ± 0.13^{Bb}	0.74 ± 0.29^{Ba}	3.52 ± 0.34^{Ab}	0.668 ± 0.071^{ABb}	0.030 ± 0.006^{Ab}	0.060 ± 0.025^{Bb}	0.522 ± 0.056^{Ab}
	40–60	3.27 ± 0.33^{Ac}	0.34 ± 0.08^{Bb}	0.60 ± 0.20^{ABa}	2.09 ± 0.34^{Ab}	0.561 ± 0.056^{Ab}	0.019 ± 0.004^{Bb}	0.033 ± 0.009^{Bb}	0.453 ± 0.043^{Ab}
Pioneer weed	0–20	12.03 ± 0.56^{Ca}	2.15 ± 0.30^{CDa}	2.43 ± 0.14^{Ca}	6.07 ± 0.33^{ABa}	1.333 ± 0.043^{Ba}	0.156 ± 0.015^{Ca}	0.333 ± 0.043^{Aa}	0.758 ± 0.020^{BCa}
(PWS)	20–40	4.98 ± 0.44^{ABb}	0.72 ± 0.14^{Bb}	0.62 ± 0.07^{Bb}	3.14 ± 0.24^{Ab}	0.796 ± 0.100^{Ab}	0.044 ± 0.010^{Ab}	0.093 ± 0.027^{Bb}	0.607 ± 0.063^{Ab}
	40–60	3.66 ± 0.35^{Ab}	0.28 ± 0.04^{Bb}	0.46 ± 0.03^{Bb}	2.55 ± 0.28^{Ab}	0.572 ± 0.042^{Ac}	0.016 ± 0.003^{Bb}	0.043 ± 0.008^{Bb}	0.471 ± 0.031^{Ac}
Herb	0–20	8.15 ± 0.32 ^{Da}	1.47 ± 0.12 ^{Da}	1.45 ± 0.12 ^{Da}	4.31 ± 0.27^{Ba}	1.007 ± 0.066^{Ca}	0.085 ± 0.003 ^{Da}	0.137 ± 0.011^{Ba}	0.670 ± 0.048^{Ca}
(HS)	20–40	4.07 ± 0.29^{Bb}	0.50 ± 0.02^{Bb}	0.39 ± 0.11^{Bb}	2.73 ± 0.18^{Ab}	0.633 ± 0.094^{ABb}	0.027 ± 0.003^{Ab}	0.064 ± 0.040^{Bab}	0.472 ± 0.042^{Ab}
	40–60	3.44 ± 0.12^{Ab}	0.35 ± 0.08^{Bb}	0.35 ± 0.07^{Bb}	2.40 ± 0.09^{Ab}	0.560 ± 0.029^{Ab}	0.019 ± 0.005^{Bb}	0.034 ± 0.009^{Bb}	0.445 ± 0.038^{Ab}
Shrub	0–20	11.94 ± 1.00^{Ca}	3.29 ± 0.63^{Ca}	2.78 ± 0.40^{Ca}	5.75 ± 1.25^{ABa}	1.322 ± 0.094^{Ba}	0.261 ± 0.011^{Ba}	0.357 ± 0.050^{Aa}	0.667 ± 0.077^{Ca}
(SS)	20–40	5.10 ± 0.65^{ABb}	0.52 ± 0.19^{Bb}	0.81 ± 0.06^{Bb}	3.57 ± 0.49^{Aab}	0.679 ± 0.081^{ABb}	0.044 ± 0.015^{Ab}	0.083 ± 0.008^{Bb}	0.528 ± 0.061^{Aab}
	40–60	3.90 ± 0.76^{Ab}	0.62 ± 0.18^{Bb}	0.57 ± 0.06^{ABb}	2.55 ± 0.58^{Ab}	0.534 ± 0.052^{Ab}	0.040 ± 0.012^{Ab}	0.055 ± 0.006^{ABb}	0.419 ± 0.038^{Ab}
Early forest	0–20	16.77 ± 1.07^{Ba}	5.19 ± 0.50^{Ba}	4.05 ± 0.34^{Ba}	7.37 ± 0.71^{Aa}	1.656 ± 0.085^{Aa}	0.323 ± 0.038^{Ba}	0.354 ± 0.024^{Aa}	0.888 ± 0.054^{ABa}
(EFS)	20–40	4.43 ± 0.33^{ABb}	0.92 ± 0.12^{Bb}	0.50 ± 0.06^{Bb}	2.91 ± 0.36^{Ab}	0.546 ± 0.041^{Bb}	0.031 ± 0.005^{Ab}	0.040 ± 0.003^{Bb}	0.445 ± 0.038^{Ab}
	40–60	3.24 ± 0.41^{Ab}	0.51 ± 0.05^{Bb}	0.45 ± 0.05^{Bb}	2.20 ± 0.35^{Ab}	0.588 ± 0.095^{Ab}	0.026 ± 0.005^{ABb}	0.051 ± 0.009^{ABb}	0.476 ± 0.082^{Ab}
Climax forest	0–20	21.76 ± 1.26^{Aa}	7.76 ± 0.67^{Aa}	5.52 ± 0.36^{Aa}	8.15 ± 1.31^{Aa}	1.854 ± 0.089^{Aa}	0.419 ± 0.032^{Aa}	0.398 ± 0.040^{Aa}	0.999 ± 0.046^{Aa}
(CFS)	20–40	5.94 ± 0.51^{Ab}	1.57 ± 0.13^{Ab}	1.57 ± 0.43^{Ab}	2.67 ± 0.43^{Ab}	0.737 ± 0.032^{ABb}	0.057 ± 0.007^{Ab}	0.232 ± 0.030^{Ab}	0.428 ± 0.057^{Ab}
	40–60	4.52 ± 0.06^{Ab}	1.30 ± 0.20^{Ab}	0.82 ± 0.11^{Ab}	2.26 ± 0.35^{Ab}	0.572 ± 0.031^{Ab}	0.034 ± 0.005^{ABb}	0.077 ± 0.016^{Ac}	0.439 ± 0.027^{Ab}

Different superscript upper-case letters imply statistically significant differences at the α = 0.05 level between revegetation stages at the same soil depth. Different superscript lower-case letters imply statistically significant differences at the α = 0.05 level between soil depths at the same revegetation stage. See Table 1 for abbreviations.

up 71.23–82.24% of the bulk weight of the soil (Fig. 4) but comprised 37.00–70.00% of the SOM-C content, and 50.24–82.34% of the SOM-N content across revegetation stages (Fig. 5c, f). The percentage of soil mass decreased from MAOM, to IPOM, and to FLF in the 0–60 cm soil layers for each revegetation stage (Fig. 4). The percentage of FLF mass (0–20 cm) progressively raised along with natural revegetation (Fig. 4a). The percentages of IPOM and MAOM mass (0–40 cm) changed little along with natural revegetation (Fig. 4a and b).

The FLF-C/SOM-C in the 0–60 cm soil layers, and IPOM-C/SOM-C in the 0–40 cm soil layers progressively increased along with natural revegetation (Fig. 5a and b). The MAOM-C/SOM-C in the 0–20 cm soil layer gradually reduced along with natural revegetation, and which in the 20–40 cm soil layer was lowest in the climax forest between revegetation stages (Fig. 5c). The FLF-N/SOM-N in the 0–20 cm soil layer of the climax and early forests, and shrub stages was markedly greater than that of the herb, pioneer weed, and farmland stages (Fig. 5d). The IPOM-N/SOM-N in the 0–20 cm soil layer was highest in the climax and early forests, shrub, and pioneer weed stages, and in the 20–60 cm soil layer was highest in the climax forest (Fig. 5e). The MAOM-N/SOM-N in the 0–20 cm soil layer was highest in the farmland and herb stage, and in the 20–40 cm soil layer was lowest in the climax forest (Fig. 5f).

3.4. Natural stable isotope abundance of SOM fractions

Natural revegetation notably affected the $\delta^{13}C$ and $\delta^{15}N$ values of SOM, FLF, IPOM, MAOM (Table 1). The $\delta^{13}C$ value of SOM, FLF, and IPOM in the 0–60 cm soil layer were greatest in the farmland between revegetation stages (Table 3). The $\delta^{13}C$ value of SOM in the 0–20 cm soil layer was lowest in the early and climax forests (Table 3). The SOM and IPOM (20–60 cm), and FLF (40–60 cm) of the climax and early forests, shrub, herb, and pioneer weed stages were significantly ($P < 0.05$) more depleted in $\delta^{13}C$ than were those of the farmland (Table 3). The $\delta^{13}C$ value of MAOM (0–20 cm) changed little along with natural revegetation (Table 3). The SOM in the 0–20 cm soil layer of farmland and herb stages were significantly ($P < 0.05$) more enriched in $\delta^{13}C$ than were those of shrub, early and climax forests (Table 3). The FLF, IPOM, and MAOM in the 0–20 cm soil layer of farmland were significantly ($P < 0.05$) more enriched in $\delta^{15}N$ than were those of the other revegetation stages (Table 3). The $\delta^{13}C$ and $\delta^{15}N$ values decreased from MAOM, to SOM, IPOM, and FLF (Table 3). Moreover, $\delta^{13}C$ and $\delta^{15}N$ values of SOM, FLF, IPOM, MAOM were clearly impacted by soil depth (Table 1). The $\delta^{13}C$ and $\delta^{15}N$ values of SOM, FLF, IPOM, MAOM in the 0–20 cm soil layer were considerably more depleted than those in the 20–60 cm soil layers for each revegetation stage, with very few exceptions (Table 3).

3.5. Linking SOM fractions to plant and soil characteristics

Pearson's correlation analysis revealed that the C and N concentrations of SOM, FLF, IPOM, and FLF-C/SOM-C, IPOM-C/SOM-C, FLF-N/SOM-N, IPOM-N/SOM-N, C:N ratio of SOM, MBC, and MBN (0–60 cm) across revegetation stages were all significantly positively ($P < 0.05$) associated with litter and root biomass (Table 4). MAOM-C/SOM-C and MAOM-N/SOM-N displayed significant negative correlation with litter and root biomass (Table 4). The $\delta^{13}C$ value of SOM, FLF, MAOM, and $\delta^{15}N$ value of FLF, MAOM-C/SOC, and MAOM-N/SOM-N across revegetation stages had negative correlation significantly ($P < 0.05$) with litter biomass (Table 4). The $\delta^{13}C$ and $\delta^{15}N$ values of SOM, FLF, IPOM, MAOM, and MAOM-C/SOM-C, MAOM-N/SOM-N across revegetation stages had significant negative correlations with root biomass (Table 4). The C and N concentrations of SOM, FLF, IPOM, and MAOM, and C:N ratios of SOM and MAOM across revegetation stages show positive relationship significantly ($P < 0.01$) with one another. Further, they all demonstrated substantial positive associations with the soil moisture, MBC, MBN, and were significantly ($P < 0.01$) adversely correlated with the soil pH and BD (Table 4). The $\delta^{13}C$ and $\delta^{15}N$ values of SOM, FLF, IPOM, and MAOM across revegetation stages were significantly ($P < 0.05$) positively related to soil pH and BD; however, they were substantially adversely correlated with soil moisture, MBC, MBN, and the C and N concentrations of SOM, FLF, and IPOM (Table 4). The FLF-C/SOM-C, IPOM-C/SOC, FLF-N/SOM-N, and IPOM-N/SOM-N ratios were substantially positively associated with soil moisture, MBC, MBN, C and N concentrations of SOM, FLF, and IPOM, which were strongly adversely related to the soil pH (Table 4).

4. Discussion

Natural revegetation markedly promoted organic C and TN accumulation in SOM and its fractions in the surface soil (0–20 cm) on the Loess Plateau of China (Table 2; Fig. 2). The concentrations and stocks of C and N in SOM and its fractions of the surface soil did not obviously increase during the early stages of revegetation (i.e., pioneer weed, herb, and shrub stages), while they were greatly enhanced during the later stages of revegetation (i.e., early and climax forests) (Table 2; Fig. 2).

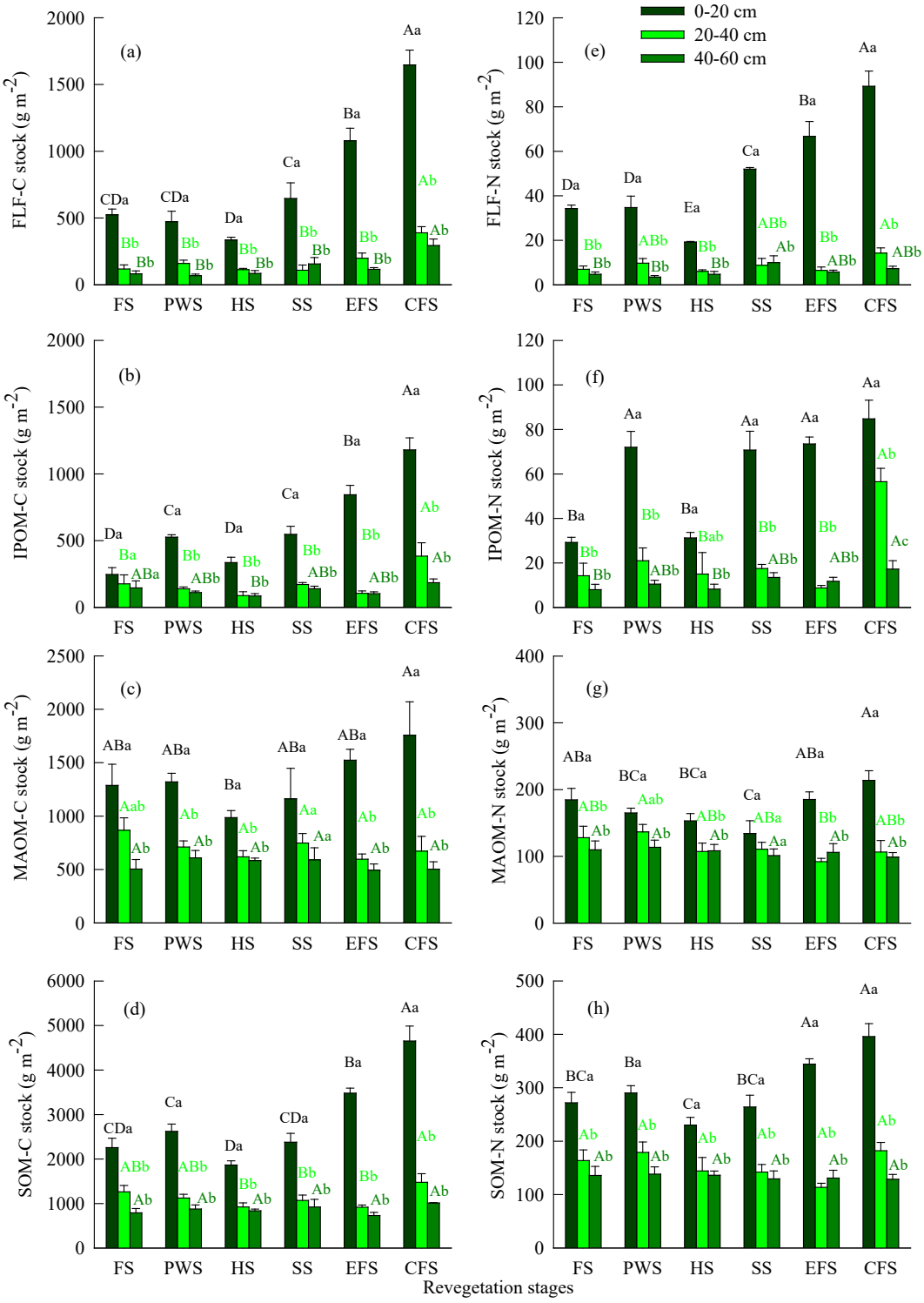

Fig. 2. The organic C and total N stocks (mean ± SE, n = 4) in SOM fractions during different revegetation stages on the Loess Plateau of China. Various superscript upper-case letters imply statistically significant differences at the α = 0.05 level between revegetation stages at the same soil depth. Various superscript lower-case letters imply statistically significant differences at the α = 0.05 level between soil depths at the same revegetation stage. FS: Farmland stage; PWS: Pioneer weed stage; HS: Herb stage; SS: Shrub stage; EFS: Early forest stage; and CFS: Climax forest stage. See Table 1 for abbreviations.

The greatest C and N stocks in SOM in the surface soil of the climax forest were mainly resulted from an increase in C and N in FLF and IPOM (Fig. 2). This finding was similar with Wang et al. (2021) who reported that enhanced total SOC pools along with post-agricultural restoration was primarily derived from increments of non-protected C. The FLF is non-protected OM, and is primarily comprised of undegraded and partially decayed plant residues (Christensen, 1992; Francisco et al., 2021), including unattached particles of litter and root material (Dietterich et al., 2021), spores, and fungal hyphae (Modak et al., 2020). The IPOM is also largely comprised of new and partly decayed plant residues (Samson et al., 2020); however, it is physically protected by soil aggregates (Kauer et al., 2021). In this study, the biomass of litter and root

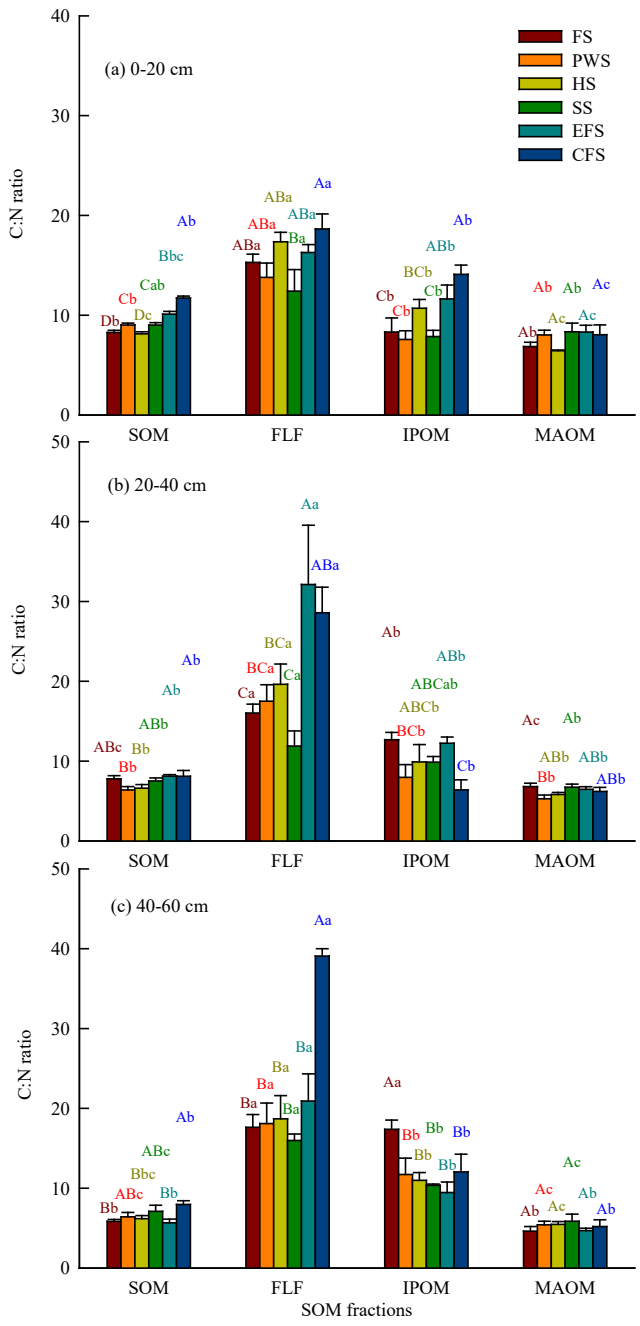

Fig. 3. The C:N ratio (mean ± SE, n = 4) of SOM, FLF, IPOM, and MAOM during different revegetation stages on the Loess Plateau of China. Various upper-case letters over the bars imply statistically significant differences at the α = 0.05 level between revegetation stages in each soil fraction. Various lower-case letters over the bars imply statistically significant differences at the α = 0.05 level between SOM fractions at each revegetation stage. See Table 1 and Fig. 2 for abbreviations.

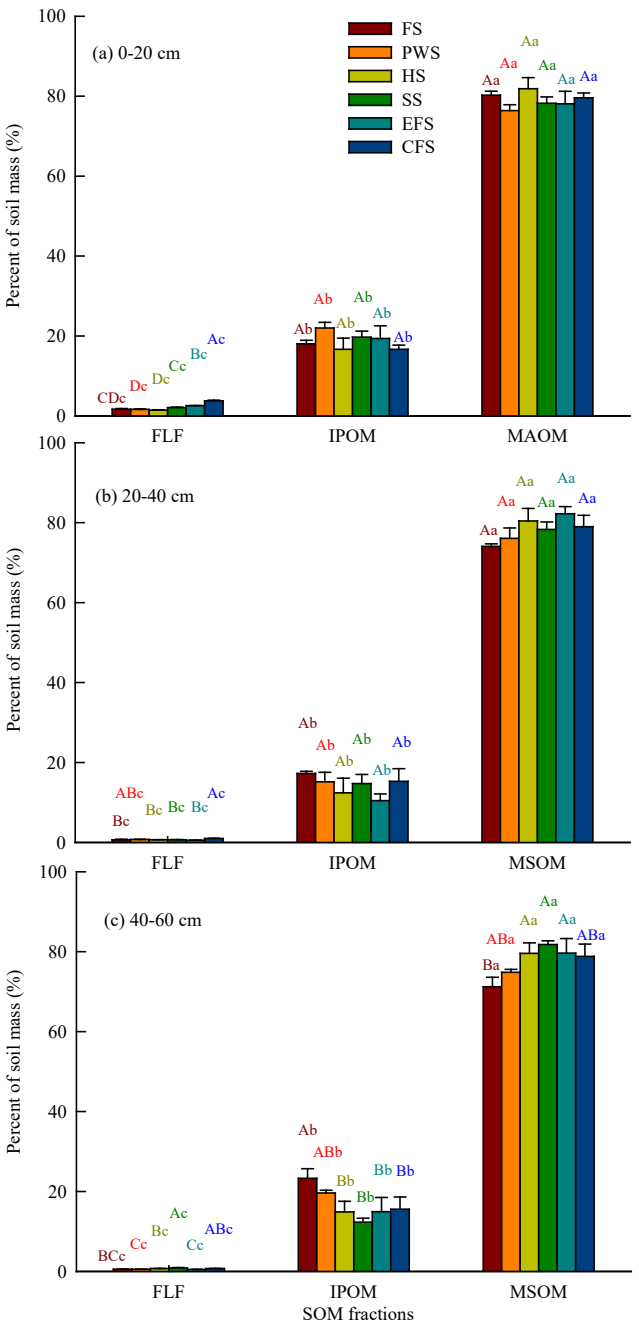

Fig. 4. Mass proportion (mean ± SE, n = 4) of FLF, IPOM, and MAOM in the bulk soil (0–20, 20–40, and 40–60 cm depths) of different revegetation stages on the Loess Plateau of China. Different supper-case letters over the bars indicate statistically significant differences at the α = 0.05 level between revegetation stages in each soil fraction. Different lower-case letters over the bars indicate statistically significant differences at the α = 0.05 level between SOM fractions in each revegetation stage. See Table 1 and Fig. 2 for abbreviations.

were progressively enhanced along with natural revegetation (Table S2; Fig. S1). It was inferred that greatly increased plant detritus (i.e., litter, roots, etc.) that as one of the most important components of FLF and IPOM entering the soil (Table S2; Fig. S1), which greatly facilitated C and N accumulation in FLF, IPOM, and the bulk SOM (0–20 cm) in the latter phases of revegetation, especially in the climax forest (Table 2; Fig. 2). This inference was supported by the result of Pearson's correlation analysis, which indicated that FLF-C, IPOM-C, FLF-N, and IPOM-N were intimately related to litter and root biomass (Table 4).

Simultaneously, increased C and N stocks in SOM of the surface soil in climax forest were partially ascribed to the enrichment of C and N in MAOM, even though their increased stocks were far lower than for FLF and IPOM (Fig. 2). MAOM has been widely recognized as the largest and most stable soil fraction, which contains the oldest C and N (Lavallee et al., 2020), owing to its tendency to bind to silt- and clay-sized mineral particles that protect it against decomposition (Santos et al., 2020). Numerous studies have documented that MAOM is microbially-derived, instead of plant-originating OM (Rocci et al., 2021), which predominantly consists of microbial residues (e.g., microbial biomass or necromass) (Prater et al., 2020), and microbial by-products derived from the

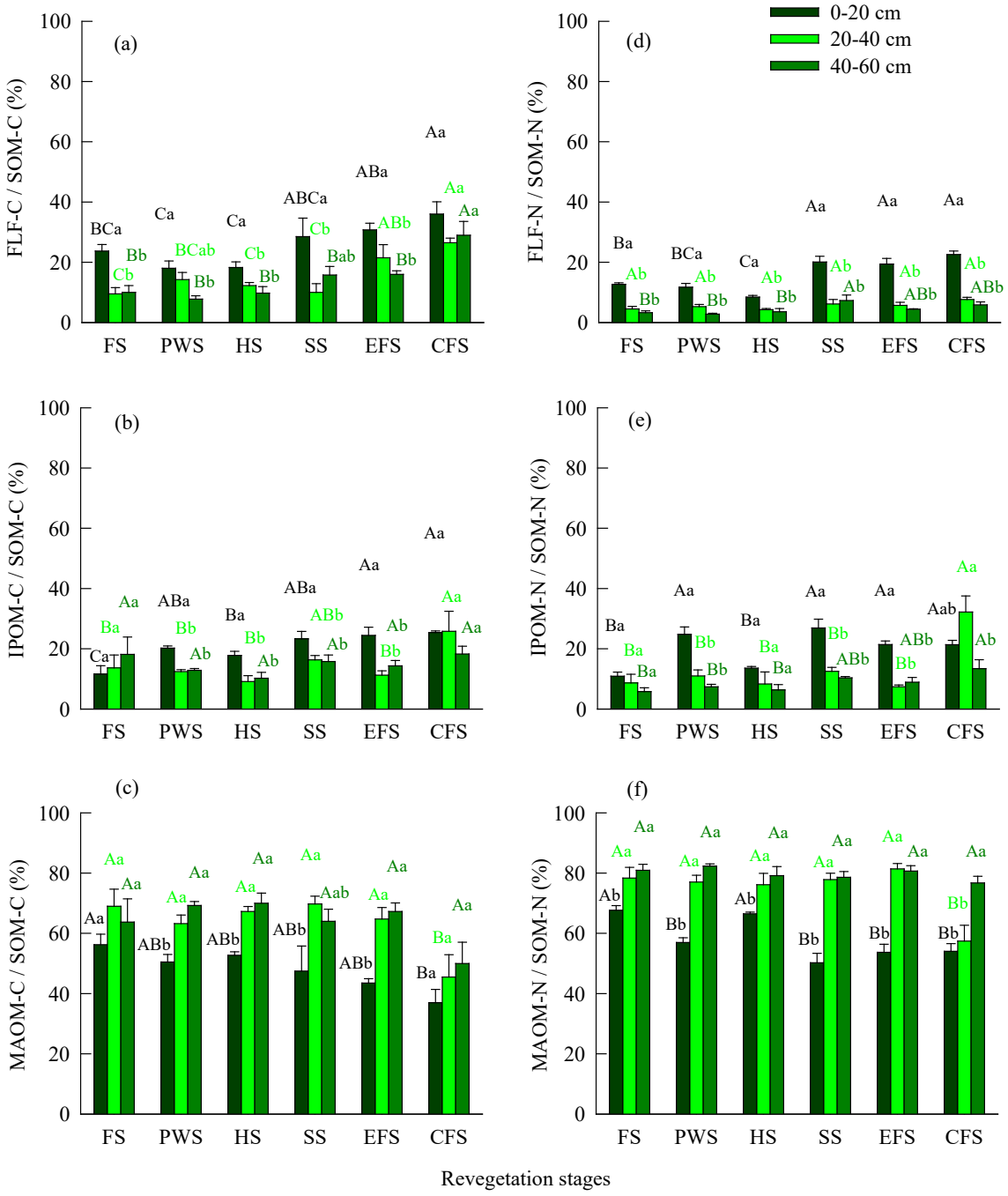

Fig. 5. The distribution proportions of C and N contents (mean ± SE, n = 15) in FLF, IPOM, and MAOM during different revegetation stages on the Loess Plateau of China. Different superscript upper-case letters indicate statistically significant differences at the α = 0.05 level between revegetation stages at the same soil depth. Different superscript lower-case letters indicate statistically significant differences at the α = 0.05 level between soil depths at the same revegetation stage. See Table 1 and Fig. 2 for abbreviations.

microbial growth, transformation, and decomposition process of OM (Plaza et al., 2016; Samson et al., 2020). It was well known that OM can be reallocated between fractions during soil physical fractionation through microbial decomposition (Angst et al., 2019). Generally, IPOM is a precursor to the formation of MAOM (Jilling et al., 2020). Soil microbes break down plant-derived IPOM, and its progressive fragmentation results in smaller, more soluble compounds that are produced by microbes, or as microbial by-products, and bound to mineral particles to eventually form finer and more stable MAOM (Craig et al., 2021). Olayemi et al. (2022) documented that MAOM increased along with enhanced IPOM decomposition. Additionally, high quality plant C inputs, particularly from root detritus and exudation, have been reported to provide abundant available substrates to microbes, and promote microbial proliferation and activity, which result in increased microbial by-products that drive MAOM formation (Sokol et al., 2019; Pierson et al., 2021). In the current study, root biomass, MBC, MBN concentrations, and the concentrations and stocks of IPOM in the surface soil progressively increased along with natural revegetation, and reached a maximum in the climax forest (Table 2 and Table S2; Fig. 2). Our results revealed that MAOM-C and MAOM-N showed positive relationship strongly with root biomass, MBC, MBN, IPOM-C, and IPOM-N (Table 4). However, MAOM-C and MAOM-N had no correlation with

Table 3
The $\delta^{13}C$ (‰) and $\delta^{15}N$ (‰) values in SOM fractions during various revegetation stages on the Loess Plateau of China.

Revegetation stages	Soil depth (cm)	$\delta^{13}C$ (‰)				$\delta^{15}N$ (‰)			
		SOM	FLF	IPOM	MAOM	SOM	FLF	IPOM	MAOM
Farmland (FS)	0–20	-21.26 ± 0.32^{Aa}	-22.69 ± 0.27^{Ab}	-22.54 ± 0.42^{Ab}	-20.84 ± 1.08^{Aa}	2.21 ± 0.18^{Ab}	0.44 ± 0.18^{Ab}	1.07 ± 0.16^{Ab}	3.94 ± 0.08^{Ab}
	20–40	-19.55 ± 0.86^{Aa}	-20.91 ± 0.55^{Aab}	-20.75 ± 0.52^{Aab}	-19.10 ± 0.80^{Aa}	4.06 ± 0.50^{ABa}	2.24 ± 0.18^{Aa}	3.06 ± 0.33^{Aa}	5.86 ± 0.17^{Aa}
	40–60	-18.87 ± 1.21^{Aa}	-20.15 ± 0.86^{Aa}	-20.08 ± 0.85^{Aa}	-18.35 ± 1.08^{Aa}	4.31 ± 0.12^{Ba}	2.58 ± 0.17^{Aa}	3.29 ± 0.19^{Aa}	6.13 ± 0.18^{Aa}
Pioneer weed (PWS)	0–20	-25.03 ± 0.12^{Cb}	-27.40 ± 0.14^{Cb}	-26.89 ± 0.12^{Cb}	-21.19 ± 0.34^{Ab}	1.61 ± 0.14^{ABb}	-1.95 ± 0.17^{BCb}	-1.14 ± 0.27^{Cb}	2.36 ± 0.13^{Bb}
	20–40	-23.40 ± 0.21^{Ba}	-25.79 ± 0.25^{BCa}	-25.28 ± 0.28^{Ba}	-19.58 ± 0.27^{Aa}	4.19 ± 0.21^{ABa}	0.75 ± 0.10^{BCa}	1.87 ± 0.13^{BCa}	4.94 ± 0.18^{Ba}
	40–60	-23.37 ± 0.17^{Ba}	-25.72 ± 0.25^{Ba}	-25.19 ± 0.23^{Ba}	-19.47 ± 0.23^{ABa}	4.53 ± 0.29^{ABa}	0.99 ± 0.10^{CDa}	2.01 ± 0.14^{Ca}	5.28 ± 0.22^{Ba}
Herb (HS)	0–20	-24.20 ± 0.07^{Bb}	-26.78 ± 0.12^{Bb}	-25.18 ± 0.45^{Bb}	-20.97 ± 0.41^{Ab}	2.23 ± 0.08^{Ab}	-1.53 ± 0.14^{Bb}	-0.35 ± 0.03^{Bb}	2.52 ± 0.13^{Bb}
	20–40	-23.12 ± 0.12^{Ba}	-25.68 ± 0.16^{BCa}	-24.11 ± 0.30^{Ba}	-19.84 ± 0.34^{ABa}	4.82 ± 0.22^{Aa}	1.11 ± 0.11^{Ba}	2.22 ± 0.10^{Ba}	5.15 ± 0.24^{Ba}
	40–60	-23.25 ± 0.17^{Ba}	-25.85 ± 0.18^{Ba}	-24.27 ± 0.11^{Bab}	-20.03 ± 0.18^{ABab}	5.06 ± 0.18^{Aa}	1.39 ± 0.09^{Ba}	2.41 ± 0.11^{BCa}	5.48 ± 0.17^{Ba}
Shrub (SS)	0–20	-25.67 ± 0.28^{CDb}	-27.41 ± 0.10^{Cb}	-26.44 ± 0.09^{Cb}	-22.49 ± 0.68^{Ab}	1.40 ± 0.22^{BCb}	-1.89 ± 0.16^{BCc}	-0.59 ± 0.11^{BCc}	1.63 ± 0.10^{Cb}
	20–40	-24.00 ± 0.26^{Ba}	-25.65 ± 0.31^{BCa}	-25.02 ± 0.27^{Ba}	-20.91 ± 0.30^{Ba}	3.60 ± 0.27^{Ba}	0.35 ± 0.05^{Cb}	1.57 ± 0.15^{Cb}	3.90 ± 0.29^{Ca}
	40–60	-23.96 ± 0.26^{Ba}	-25.39 ± 0.35^{Ba}	-24.64 ± 0.39^{Ba}	-20.74 ± 0.29^{Ba}	4.05 ± 0.15^{Ba}	0.89 ± 0.08^{Da}	2.13 ± 0.12^{Ca}	4.47 ± 0.18^{Ca}
Early forest (EFS)	0–20	-25.97 ± 0.21^{Db}	-27.86 ± 0.26^{Cb}	-26.92 ± 0.06^{Cb}	-22.60 ± 0.86^{Ab}	0.82 ± 0.31^{Cb}	-2.35 ± 0.13^{Cc}	-1.06 ± 0.11^{Cc}	1.78 ± 0.16^{Cc}
	20–40	-23.47 ± 0.80^{Ba}	-25.33 ± 0.20^{Ba}	-24.39 ± 0.48^{Ba}	-20.05 ± 0.36^{ABa}	3.77 ± 0.21^{Ba}	0.59 ± 0.11^{Cb}	1.93 ± 0.17^{BCb}	4.69 ± 0.22^{Bb}
	40–60	-23.58 ± 0.23^{Ba}	-25.54 ± 0.34^{Ba}	-24.58 ± 0.47^{Ba}	-20.34 ± 0.15^{Ba}	4.53 ± 0.28^{ABa}	1.32 ± 0.11^{BCa}	2.62 ± 0.11^{Ba}	5.53 ± 0.24^{Ba}
Climax forest (CFS)	0–20	-25.80 ± 0.25^{Db}	-27.81 ± 0.12^{Cb}	-26.11 ± 0.14^{Cb}	-22.57 ± 0.64^{Ab}	1.11 ± 0.20^{BCc}	-1.89 ± 0.19^{BCc}	0.05 ± 0.19^{Bc}	2.25 ± 0.09^{Bc}
	20–40	-24.39 ± 0.29^{Ba}	-26.48 ± 0.36^{Ca}	-25.17 ± 0.40^{Ba}	-21.24 ± 0.22^{Ba}	3.58 ± 0.12^{Bb}	0.59 ± 0.12^{Cb}	2.48 ± 0.17^{Bb}	4.73 ± 0.17^{Bb}
	40–60	-23.90 ± 0.25^{Ba}	-25.95 ± 0.33^{Ba}	-24.34 ± 0.13^{Ba}	-20.56 ± 0.21^{Ba}	4.44 ± 0.03^{ABa}	1.37 ± 0.12^{Ba}	3.41 ± 0.11^{Aa}	5.62 ± 0.14^{ABa}

Different superscript upper-case letters imply statistically significant differences at the $\alpha = 0.05$ level between revegetation stages at the same soil depth. Different superscript lower-case letters imply statistically significant differences at the $\alpha = 0.05$ level between soil depths at the same revegetation stage. See Table 1 for abbreviations.

litter biomass, which further supported previous study showing that MAOM is independent of original plant litter (Prater et al., 2020). We deduced that the highest C and N stocks in MAOM of the surface soil in the climax forest were primarily led by greatly increased C and N in IPOM, microbial biomass (i.e., MBC, MBN), and the root biomass in the climax forest that drove MAOM formation (Table 2 and Table S2; Fig. 2).

Unsurprisingly, the root biomass, C and N stocks in SOM fractions greatly decreased along soil depth increments across the entire soil profile (Table S2; Fig. 2), which aligned with earlier studies showing that the contents of C and N in SOM fractions declined with soil depth (Ojeda et al., 2018; Wuaden et al., 2020). On average, 56% of root biomass, 70% of FLF-C, 75% of FLF-N, 65% of IPOM-C, 64% of IPOM-N, 51% of MAOM-C, 44% of MAOM-N, 58% of SOM-C, and 51% of SOM-N were allocated to the surface soil across revegetation stages (Table S2; Fig. 2). This suggested that the vertical distributions of C and N in SOM fractions were largely concentrated in the surface soil rather than the deeper soil across revegetation stages. The greater allocation of C and N in SOM fractions of the surface soil for each revegetation stage relative to the deeper soil resulted primarily from a thick litter layer that covered the surface soil (Fig. 1), and most root materials distributing in the surface soil (Table S2). These abundant plant residues input into the surface soil greatly promoted C and N accumulation in the surface soil for every revegetation stage (Fig. 2; King and Hofmockel, 2017; Gabriel et al., 2018). Conversely, greatly decreased C and N in SOM fractions of the deeper soil for each restoration stage were mainly attributed to limited organic inputs (e.g., litter and root) (Table 2 and Table S1; Fig. 2). The stocks of FLF-C, IPOM-C, and IPOM-N in the 20–60 cm soil layers, and FLF-N in the 20–40 cm soil layer were highest in the climax forest (Fig. 2), which may have still been affected by the greatest litter input (Fig. S1a; Samson et al., 2020; Dietterich et al., 2021). The stocks of MAOM-C (20–60 cm) and MAOM-N (40–60 cm) remained unaffected by natural revegetation (Fig. 2), which was primarily attributed to the root biomass (Sokol et al., 2019; Pierson et al., 2021), as well as biomass of microbes (i.e., MBC and MBN; Prater et al., 2020). These were important driving factors for MAOM variations not being impacted by vegetation revegetation in deeper soil (Table S2).

Natural revegetation greatly altered the distribution and stabilization of C and N in SOM fractions (Fig. 5). The FLF is widely recognized as the freshest and most labile fraction with a rapid decomposition rate, which is not physically or chemically protected by the soil and is accessible to microbes (Yang et al., 2017; Williams et al., 2018). Conversely, the MAOM is the oldest and most persistent fraction with lower bioavailability and decomposition rates with a prolonged residency in the soil as it chemically binds to minerals (Lavallee et al., 2020; Macedo et al., 2021; Pierson et al., 2021). The IPOM has a faster decomposition rate and shorter residence time relative to those of MAOM; however, it has longer residence time compared to that of FLF due to IPOM being physically protected by soil aggregates (Six et al., 1998; Lavallee et al., 2020; Kauer et al., 2021). In this study, the distribution proportions of C in FLF (i.e., FLF-C/SOM-C) and that of N in IPOM (i.e., IPOM-N/SOM-N) (0–60 cm), and that of C in IPOM (i.e., IPOM-C/SOM-C), and that of N in FLF (i.e., FLF-N/SOM-N) in the surface soil gradually increased along with natural revegetation (Fig. 5). However, the distribution proportions of C and N in MAOM in the surface soil gradually decreased along with natural revegetation (Fig. 5). These changes implied that natural revegetation altered C and N stabilization in SOM through increasing distribution proportions of non-protected and pure physically protected C and N, and decreasing distribution proportions of chemical protected C and N (Fig. 5) (Sollins et al., 1996; Briedis et al., 2018; Wang et al., 2021). Generally, the C:N ratio decreases during decomposition of SOM, and a higher C:N ratio implies a lower SOM decomposition rate (Artemyeva et al., 2021). In present study, C:N ratio of SOM in the surface soil progressively enhanced along with natural revegetation, which was primarily the result of increased C:N ratio in FLF and IPOM (Fig. 3). The lower decomposition of FLF and IPOM in the surface soil of the climax forest (Fig. 3; Artemyeva et al., 2021) may have been primarily ascribed to higher litter C:N ratio that is resistant to decomposition in climax forest (Fig. S1). Additionally, our previous study reported that natural revegetation enhanced the inherent biochemical recalcitrance of SOC pool (Zhang et al., 2022). Santos et al. (2020) have reported that MAOM was primarily comprised of low molecular weight and low C/N ratios of labile compounds, which quickly decomposed once exposed to microbes (Lavallee et al., 2020). The MAOM as the most stable fraction, and its stability is strongly dependent on its capacity to chemically bind to minerals (Santos et al., 2020; Macedo et al., 2021). However, IPOM has been reported to exhibit a higher inherent biochemical recalcitrance (e.g., lignified material) than MAOM (Haddix et al., 2020; Kauer et al., 2021). We presumed that increased inherently biochemical recalcitrance of SOC in the climax forest (Zhang et al., 2022) might be preserved in IPOM (Kauer et al., 2021). It was deduced that natural revegetation greatly modified C and N stabilization in SOM of the surface soil by increasing the allocation of C and N in FLF and IPOM, and decreasing the C and N allocation in MAOM (Fig. 5). This may have been driven by FLF and IPOM in the

Table 4
Correlation analysis of C and N in SOM fractions and soil properties (0–60 cm) across revegetation stages on the Loess Plateau of China.

	LB	RB	pH	Moisture	BD	MBC	MBN	FLF-C	IPOM-C	MAOM-C	FLF-N	IPOM-N	MAOM-N
SOM-C	0.649**	0.773**	–0.871**	0.717**	–0.335**	0.946**	0.900**	0.929**	0.947**	0.914**	0.966**	0.882**	0.873**
FLF-C	0.608**	0.753**	–0.806**	0.743**	–0.302**	0.891**	0.822**	1	0.923**	0.721**	0.958**	0.818**	0.723**
IPOM-C	0.737**	0.725**	–0.830**	0.740**	–0.313**	0.912**	0.843**	0.923**	1	0.776**	0.927**	0.904**	0.739**
MAOM-C	0.371	0.678**	–0.810**	0.599**	–0.327**	0.846**	0.826**	0.721**	0.776**	1	0.839**	0.759**	0.911**
SOM-N	0.417*	0.737**	–0.841**	0.645**	–0.349**	0.922**	0.908**	0.886**	0.894**	0.922**	0.932**	0.885**	0.935**
FLF-N	0.577**	0.747**	–0.866**	0.732**	–0.332**	0.933**	0.883**	0.959**	0.928**	0.837**	1	0.866**	0.794**
IPOM-N	0.583**	0.621**	–0.813**	0.601**	–0.348**	0.835**	0.838**	0.815**	0.903**	0.762**	0.866**	1	0.687**
MAOM-N	0.098	0.683**	–0.722**	0.548**	–0.318**	0.815**	0.805**	0.723**	0.739**	0.911**	0.794**	0.687**	1
δ^{13}C-SOM	–0.509*	–0.376**	0.562**	–0.358**	0.327**	–0.540**	–0.526**	–0.499**	–0.582**	–0.313**	–0.513**	–0.584**	–0.327**
δ^{13}C-FLF	–0.470*	–0.303**	0.491**	–0.328**	0.276*	–0.508**	–0.504**	–0.459**	–0.539**	–0.270*	–0.458**	–0.546**	–0.299*
δ^{13}C-IPOM	–0.378	–0.317**	0.492**	–0.302**	0.306**	–0.505**	–0.505**	–0.450**	–0.552**	–0.325**	–0.473**	–0.567**	–0.339**
δ^{13}C-MAOM	–0.461*	–0.472**	0.668**	–0.409**	0.364**	–0.612**	–0.605**	–0.604**	–0.618**	–0.485**	–0.651**	–0.639**	–0.428**
δ^{15}N-SOM	–0.303	–0.698**	0.818**	–0.505**	0.337**	–0.880**	–0.898**	–0.788**	–0.868**	–0.853**	–0.859**	–0.837**	–0.791**
δ^{15}N-FLF	–0.435*	–0.617**	0.776**	–0.467**	0.354**	–0.874**	–0.895**	–0.723**	–0.840**	–0.743**	–0.787**	–0.808**	–0.719**
δ^{15}N-IPOM	0.022	–0.581**	0.701**	–0.373**	0.327**	–0.825**	–0.861**	–0.628**	–0.779**	–0.764**	–0.730**	–0.745**	–0.740**
δ^{15}N-MAOM	–0.361	–0.622**	0.795**	–0.436**	0.383**	–0.872**	–0.903**	–0.700**	–0.822**	–0.763**	–0.796**	–0.800**	–0.715**
FLF-C/SOM-C	0.465*	0.566**	–0.575**	0.486**	–0.177	0.596**	0.559**	0.778**	0.635**	0.327**	0.673**	0.611**	0.351**
IPOM-C/SOM-C	0.538**	0.346**	–0.485**	0.418**	–0.088	0.476**	0.430**	0.505**	0.680**	0.228	0.470**	0.655**	0.220
MAOM-C/SOM-C	–0.672**	–0.534**	0.563**	–0.451**	0.130	–0.617**	–0.590**	–0.727**	–0.728**	–0.311**	–0.641**	–0.716**	–0.354**
FLF-N/SOM-N	0.432*	0.711**	–0.849**	0.635**	–0.309**	0.886**	0.864**	0.912**	0.856**	0.742**	0.956**	0.833**	0.690**
IPOM-N/SOM-N	0.570**	0.388**	–0.587**	0.375**	–0.213	0.520**	0.558**	0.533**	0.655**	0.410**	0.544**	0.848**	0.314**
MAOM-N/SOM-N	–0.681**	–0.588**	0.753**	–0.505**	0.254*	–0.772**	–0.798**	–0.758**	–0.816**	–0.624**	–0.796**	–0.935**	–0.554**
C:N ratio-SOM	0.719**	0.702**	–0.756**	0.602**	–0.317**	0.801**	0.751**	0.814**	0.815**	0.746**	0.800**	0.735**	0.588**
C:N ratio-FLF	0.629**	–0.089	0.269*	–0.054	0.099	–0.256*	–0.316**	–0.062	–0.152	–0.397**	–0.247*	–0.199	–0.407**
C:N ratio-IPOM	–0.072	–0.004	0.126	0.073	0.061	0.021	–0.106	0.050	0.081	–0.107	–0.020	–0.258*	–0.096
C:N ratio-MAOM	0.374	0.496**	–0.672**	0.432**	–0.320**	0.650**	0.657**	0.507**	0.579**	0.836**	0.638**	0.645**	0.569**

See Table 1 for abbreviations.
* $P < 0.05$;
** $P < 0.01$.

climax forest being recalcitrant to decomposition, which slowed the formation of MAOM in the surface soil (Fig. 3; Jilling et al., 2020; Olayemi et al., 2022).

Natural revegetation significantly ($P < 0.001$) altered the δ^{13}C and δ^{15}N stable isotope signature between SOM fractions (Table 1), and affected the turnover of C and N (Table 3). In this study, the δ^{13}C value of SOM, FLF, and IPOM (0–60 cm) were most enriched in the farmland in contrast to the other revegetation stages (Table 3), which could be because of the δ^{13}C value of FLF and IPOM being akin to the existing standing vegetation (Midwood et al., 2021). Abundant maize straw produced by C_4 plants was returned to the farmland soil, which typically possessed a mean δ^{13}C value of –11‰ to –14‰ (Zhang et al., 2022). The changes in δ^{13}C value were widely employed to track the incorporation of photosynthetically fixed C into SOM fractions (Midwood et al., 2021). We found that the δ^{13}C value gradually increased with SOM decomposition from FLF, to IPOM, and to MAOM for each soil depth of each revegetation stage (Table 3), which agreed with earlier studies (Plaza et al., 2016; Midwood et al., 2021). In this study, gradually decreasing C:N ratio, from FLF, to IPOM, and to MAOM further confirmed the progressively increased decomposition of SOM (Fig. 3). Microbial processing may result in ^{13}C-enrichment in soil C (Ehleringer et al., 2000), as bacteria prefer to metabolize ^{12}C-rich compounds (Balesdent et al., 1987; Plaza et al., 2016), ultimately leading to more ^{12}C loss through soil respiration, whereas ^{13}C is retained during the decomposition of SOM (Midwood et al., 2021). Simultaneously, microbes have been reported to prefer to use ^{14}N during SOM decomposition (Nadelhoffer and Fry, 1994; Plaza et al., 2016); thus, enriching δ^{15}N in soil and losing more ^{14}N to the ambient atmosphere from FLF, to IPOM, and to MAOM for each soil depth of each revegetation stage (Table 3; Plaza et al., 2016; Prater et al., 2020). Additionally, δ^{13}C and δ^{15}N values in SOM, FLF, IPOM, and MAOM became more enriched in deeper soil (20–60 cm) than the surface soil (0–20 cm) with very few exceptions (Table 3). This has been suggested to result from the enhanced distribution ratio of C and N in MAOM (20–60 cm), which implied an increased SOM decomposition in deeper soil (Fig. 5c and f). This resulted in the loss of ^{12}C and ^{14}N, and enrichment of δ^{13}C and δ^{15}N under microbial processing (Plaza et al., 2016; Midwood et al., 2021). Generally, increases in δ^{15}N value occurred with increased N decomposition and higher N loss (Prater et al., 2020). The most enriched δ^{15}N value in SOM, FLF, and IPOM were exhibited in the farmland implying that the soil N cycle of the farmland was more open to N losses, which was largely in the form of gaseous N via nitrification and denitrification in contrast to the other revegetation stages (Table 3; Prater et al., 2020). This deduction was backed by our observation that a lower C:N ratio of SOM in the farmland indicated greater SOM decomposition (Fig. 3; Artemyeva et al., 2021), which primarily resulted from a lower litter C:N ratio in farmland in contrast to the other revegetation stages (Fig. S1).

5. Conclusions

Natural revegetation over ~ 160 years greatly promoted C and N sequestration in SOM, primarily through C and N accumulation in FLF and IPOM, as well as slow increasing C and N content of MAOM in the surface soil during later revegetation stages. The distribution proportions of C and N in FLF and IPOM increased, while that in MAOM decreased along natural revegetation in the surface soil. The δ^{13}C and δ^{15}N values gradually increased with the decomposition of SOM and soil depths for each revegetation stage. The more enriched δ^{15}N value of SOM fractions and lower C:N ratio of SOM in the farmland implied that soil N cycle was more vulnerable to the loss of N in conjunction with higher SOM decomposition in the farmland. Our results suggested that natural revegetation played an essential role in C and N sinks through the enhancement of C and N sequestration in SOM and its fractions of the topsoil, and greatly altered the C and N stabilization in SOM in the surface soil through increasing relative distribution of non-protected and pure physically protected C and N, and decreasing relative distribution of chemical protected C and N, respectively. This study represents a step forward in understanding of the variations and driving patterns of C and N in SOM following natural revegetation, and it provides scientific basis for the evaluation of ecological rejuvenation practices and soil C and N management in degraded ecosystems.

Declaration of Competing Interest

The authors declare that they have no known competing financial interests or personal relationships that could have appeared to influence the work reported in this paper.

Acknowledgements

This study was supported by the National Natural Science Foundation of China (grant no. 32071632; 31600427), the Natural Science Foundation of Shaanxi Province, China (grant no. 2022JM-114; 2019JQ-666), and the Fundamental Research Funds for the Central Universities (grant no. GK202003051), We thank Fusheng Zhao for assisting with this study.

Appendix A. Supplementary material

Supplementary data to this article can be found online at https://doi.org/10.1016/j.catena.2022.106647.

References

Angst, G., Mueller, K.E., Eissenstat, D.M., Trumbore, S., Freeman, K.H., et al., 2019. Soil organic carbon stability in forests: distinct effects of tree species identity and traits. Global Change Biol. 25, 1529–1546.

Artemyeva, Z., Danchenko, N., Kolyagin, Y., Kirillova, N., Kogut, B., 2021. Chemical structure of soil organic matter and its role in aggregate formation in Haplic Chernozem under the contrasting land use variants. Catena 204, 105403.

Atere, C.T., Gunina, A., Zhu, Z.K., Xiao, M.L., Liu, S.L., 2020. Organic matter stabilization in aggregates and density fractions in paddy soil depending on long-term fertilization: tracing of pathways by ^{13}C natural abundance. Soil Biol. Biochem. 149, 107931.

Ayoubi, S., Khormali, F., Sahrawat, K.L., Rodrigues, C., de Lima, A., 2011. Assessment of soil quality indicators related to land use change in a loessial soil using factor analysis in Golestan province, northern Iran. J. Agr. Sci. Tech-IRAN 13, 727–742.

Ayoubi, S., Sadeghi, N., Afshar, F.A., Abdi, M.R., Zeraatpisheh, M., Rodrigo-Comino, J., 2021. Impacts of oak deforestation and rainfed cultivation on soil redistribution processes across hillslopes using Cs-137 techniques. For. Ecosyst. 8, 32.

Balesdent, J., Mariotti, A., Guillet, B., 1987. Natural 13C abundance as a tracer for studies of soil organic matter dynamics. Soil Biol. Biochem. 19, 25–30.

Baker, S., Eckerberg, K., 2016. Ecological restoration success: a policy analysis understanding. Restor. Ecol. 24, 284–290.

Briedis, C., Sá, J.C.D., Lal, R., Tivet, F., Franchini, J.C., et al., 2018. How does no-till deliver carbon stabilization and saturation in highly weathered soils? Catena 163, 13–23.

Cai, X.W., Zhang, D., Wang, Y.Q., Diao, L.F., Cheng, X.L., Luo, Y.Q., An, S.Q., Yang, W., 2022. Shift in soil microbial communities along ~160 years of natural vegetation restoration on the Loess Plateau of China. Appl. Soil Ecol. 173, 104394.

Chen, C., 1954. The vegetation and its roles in soil and water conservation in the secondary forest area in the boundary of Shaanxi and Gansu provinces. Acta Phytoecol. Geobot. Sin. 2, 152–153.

Chen, Y.X., Wei, T.X., Ren, K., Sha, G.L., Guo, X., Fu, Y.C., Yu, H., 2022. The coupling interaction of soil organic carbon stock and water storage after vegetation restoration on the Loess Plateau. China. J. Environ. Manage. 306, 114481.

Christensen, B.T., 1992. Physical fractionation of soil and organic matter in primary particle size and density separates. Adv. Soil Sci. 20, 1–90.

Craig, M.E., Mayes, M.A., Sulman, B.N., Walker, A.P., 2021. Biological mechanisms may contribute to soil carbon saturation patterns. Global Change Biol. 27, 2633–2644.

Crouzeilles, R., Curran, M., Ferreira, M.S., Lindenmayer, D.B., Grelle, C.E.V., Benayas, J. M.R., 2016. A global meta-analysis on the ecological drivers of forest restoration success. Nat. Commun. 7, 11666.

Deng, L., Liu, G.B., Shuangguan, Z.P., 2014. Land-use conversion and changing soil carbon stocks in China's 'Grain-for-Green' Program: a synthesis. Global Change Biol. 20, 3544–3556.

Deng, L., Wang, G.L., Liu, G.B., Shuangguan, Z.P., 2016. Effects of age and land-use changes on soil carbon and nitrogen sequestrations following cropland abandonment on the Loess Plateau. China. Ecol. Eng. 90, 105–112.

Deng, L., Wang, K.B., Chen, M.L., Shuangguan, Z.P., Sweeney, S., 2013. Soil organic carbon storage capacity positively related to forest succession on the Loess Plateau, China. Catena 110, 1–7.

Dietterich, L.H., Karpman, J., Neupane, A., Ciochina, M., Cusack, D.F., 2021. Carbon content of soil fractions varies with season, rainfall, and soil fertility across a lowland tropical moist forest gradient. Biogeochemistry 155, 431–452.

Ehleringer, J.R., Buchmann, N., Flanagan, L.B., 2000. Carbon isotope ratios in belowground carbon cycle processes. Ecol. Appl. 10, 412–422.

Feyissa, A., Yang, F., Feng, J., Wu, J.J., Chen, Q., Cheng, X.L., 2020. Soil labile and recalcitrant carbon and nitrogen dynamics in relation to functional vegetation groups along precipitation gradients in secondary grasslands of South China. Environ. Sci. Pollut. Res. 27, 10528–10540.

Francisco, C.A.L., Loss, A., Brunetto, G., Gonzatto, R., Giacomini, S.J., et al., 2021. Carbon and nitrogen in particle-size fractions of organic matter of soils fertilised with surface and injected applications of pig slurry. Soil Res. 60, 65–72.

Fu, B.J., Liu, Y., Lu, Y.H., He, C.S., Zeng, Y., et al., 2011. Assessing the soil erosion control service of ecosystems change in the Loess Plateau of China. Ecol. Complex 8, 284–293.

Gabriel, C.E., Kellman, L., Prest, D., 2018. Examining mineral-associated soil organic matter pools through depth in harvested forest soil profiles. PLoS ONE 13, e0206847. https://doi.org/10.1371/journal.pone.0206847.

Gao, G.Y., Tuo, D.F., Han, X.Y., Jiao, L., Li, J.R., Fu, B.J., 2020. Effects of land-use patterns on soil carbon and nitrogen variations along revegetated hillslopes in the Chinese Loess Plateau. Sci. Total Environ. 746, 141156.

Haddix, M.L., Gregorich, E.G., Helgason, B.L., Janzen, H., Ellert, B.H., Cotrufo, M.F., 2020. Climate, carbon content, and soil texture control the independent formation and persistence of particulate and mineral-associated organic matter in soil. Geoderma 363, 114160.

Han, X.Y., Gao, G.Y., Li, Z.S., Chang, R.Y., Jiao, L., Fu, B.J., 2019. Effects of plantation age and precipitation gradient on soil carbon and nitrogen changes following afforestation in the Chinese Loess Plateau. Land Degrad. Dev. 30, 2298–2310.

Hancock, G.R., Kunkel, V., Wells, T., Martinez, C., 2019. Soil organic carbon and soil erosion–Understanding change at the large catchment scale. Geoderma 343, 60–71.

Jilling, A., Kane, D., Williams, A., Yannarell, A.C., Davis, A., 2020. Rapid and distinct responses of particulate and mineral-associated organic nitrogen to conservation tillage and cover crops. Geoderma 359, 114001.

Karchegani, P.M., Ayoubi, S., Lu, S.G., Honarju, N., 2011. Use of magnetic measures to assess soil redistribution following deforestation in hilly region. J. Appl. Geophys. 75, 227–236.

Karchegani, P.M., Ayoubi, S., Mosaddeghi, M.R., Honarjoo, N., 2012. Soil organic carbon pools in particle-size fractions as affected by slope gradient and land use change in hilly regions, western Iran. J. MT. Sci.-Engl. 9, 87–95.

Kauer, K., Pärnpuu, S., Talgre, L., Eremeev, V., Luik, A., 2021. Soil particulate and mineral-associated organic matter increases in organic farming under cover cropping and manure addition. Agriculture 11, 903.

Khorchani, M., Nadal-Romero, E., Lasanta, T., Tague, C., 2022. Carbon sequestration and water yield tradeoffs following restoration of abandoned agricultural lands in Mediterranean mountains. Environ. Res. 207, 112203.

Khormali, F., Ajami, M., Ayoubi, S., Srinivasarao, C.h., Wani, S.P., 2009. Role of deforestation and hillslope position on soil quality attributes of loess-derived soils in Golestan province, Iran. Agr. Ecosyst. Environ. 134, 178–189.

King, A.E., Hofmockel, K.S., 2017. Diversified cropping systems support greater microbial cycling and retention of carbon and nitrogen. Agr. Ecosyst. Environ. 240, 66–76.

Kramer, M.G., Lajtha, K., Aufdenkampe, A.K., 2017. Depth trends of soil organic matter C: N and ^{1}5N natural abundance controlled by association with minerals. Biogeochemistry 136, 237–248.

Krishna, M., Gupta, S., Delgado-Baquerizo, M., Morriën, E., Garkoti, S.C., et al., 2020. Successional trajectory of bacterial communities in soil are shaped by plant-driven changes during secondary succession. Sci. Rep. 10, 9864.

Lavallee, J.M., Soong, J.L., Cotrufo, M.F., 2020. Conceptualizing soil organic matter into particulate and mineral-associated forms to address global change in the 21st century. Global Change Biol. 26, 261–273.

Lv, P., Sun, S.S., Medina-Roldánd, E., Zhao, S.L., Hu, Y., Guo, A.S., Zuo, X.A., 2021. Effects of habitat types on the dynamic changes in allocation in carbon and nitrogen storage of vegetation-soil system in sandy grasslands: how habitat types affect C and N allocation? Ecol. Evol. 11, 9079–9091.

Macedo, I., Pravia, M.V., Castillo, J., Terra, J.A., 2021. Soil organic matter in physical fractions after intensification of irrigated rice-pasture rotation systems. Soil Till. Res. 213, 105160.

Marín-Spiotta, E., Swanston, C.W., Torn, M.S., Silver, W.L., Burton, S.D., 2008. Chemical and mineral control of soil carbon turnover in abandoned tropical pastures. Geoderma 143, 49–62.

Midwood, A.J., Hannam, K.D., Gebretsadikan, T., Emde, D., Jones, M.D., 2021. Storage of soil carbon as particulate and mineral associated organic matter in irrigated woody perennial crops. Geoderma 403, 115185.

Minick, K.J., Leggett, Z.H., Sucre, E.B., Fox, T.R., Strahm, B.D., 2021. Bioenergy production effects on SOM with depth of loblolly pine forests on Paleaquults in southeastern USA. Geoderma Reg. 27, e00428.

Minnemeyer, S., Laestadius, L., Sizer, N., Saint-Laurent, C., Potapov, P., 2011. A world of opportunity www.forestlandscaperestoration.org.

Modak, K., Biswas, D.R., Ghosh, A., Pramanik, P., Das, T.K., 2020. Zero tillage and residue retention impact on soil aggregation and carbon stabilization within aggregates in subtropical India. Soil Till. Res. 202, 104649.

Nadelhoffer, K.J., Fry, B., 1994. N isotope studies in forested ecosystems. In: Lajtha, K., Michener, R.H. (Eds.), Stable isotopes in ecology and environmental science. Blackwell, Oxford, UK, pp. 22–44.

Ojeda, J.J., Caviglia, O.P., Agnusdei, M.G., 2018. Vertical distribution of root biomass and soil carbon stocks in forage cropping systems. Plant Soil 423, 175–191.

Olayemi, O.P., Kallenbach, C.M., Wallenstein, M.D., 2022. Distribution of soil organic matter fractions are altered with soil priming. Soil Biol. Biochem. 164, 108494.

Pierson, D., Evans, L., Kayhani, K., Bowden, R.D., Nadelhoffer, K., et al., 2021. Mineral stabilization of soil carbon is suppressed by live roots, outweighing influences from litter quality or quantity. Biogeochemistry 154, 433–449.

Pinheiro, E.F.M., de Campos, D.V.B., Balieiro, F.D., dos Anjos, L.H.C., Pereira, M.G., 2015. Tillage systems effects on soil carbon stock and physical fractions of soil organic matter. Agr. Syst. 132, 35–39.

Plaza, C., Giannetta, B., Fernández, J.M., López-de-Sá, E.G., Polo, A., Gascó, G., Méndez, A., Zaccone, C., 2016. Response of different soil organic matter pools to biochar and organic fertilizers. Agr. Ecosyst. Environ. 225, 150–159.
Prater, I., Zubrzycki, S., Buegger, F., Zoor-Füllgraff, L.C., Angst, G., Dannenmann, M., Mueller, C.W., 2020. From fibrous plant residues to mineral-associated organic carbon–the fate of organic matter in Arctic permafrost soils. Biogeosciences 17, 3367–3383.
Rocci, K.S., Lavallee, J.M., Stewart, C.E., Cotrufo, M.F., 2021. Soil organic carbon response to global environmental change depends on its distribution between mineral-associated and particulate organic matter: a meta-analysis. Sci. Total Environ. 793, 148569.
Rosenzweig, S.T., Carson, M.A., Baer, S.G., Blair, J.M., 2016. Changes in soil properties, microbial biomass, and fluxes of C and N in soil following post-agricultural grassland restoration. Appl. Soil Ecol. 100, 186–194.
Samson, M.E., Chantigny, M.H., Vanasse, A., Menasseri-Aubry, S., Angers, D.A., 2020. Coarse mineral-associated organic matter is a pivotal fraction for SOM formation and is sensitive to the quality of organic inputs. Soil Biol. Biochem. 149, 107935.
Santos, R.S., Oliveira, F.C.C., Ferreira, G.W.D., Ferreira, M.A., Araújo, E.F., Silva, I.R., 2020. Carbon and nitrogen dynamics in soil organic matter fractions following eucalypt afforestation in southern Brazilian grasslands (*Pampas*). Agr. Ecosyst. Environ. 301, 106979.
Six, J., Elliott, E.T., Paustian, K., Doran, J.W., 1998. Aggregation and soil organic matter accumulation in cultivated and native grass soils. Soil Sci. Soc. Am. J. 62, 1367–1377.
Skjemstad, J.O., Le Feuvre, R.P., Prebble, R.E., 1990. Turnover of soil organic matter under pasture as determined by ^{13}C natural abundance. Soil Fertil. Plant Nutr. 28, 267–276.
Sokol, N.W., Kuebbing, S.E., Karlsen-Ayala, E., Bradford, M.A., 2019. Evidence for the primacy of living root inputs, not root or shoot litter, in forming soil organic carbon. New Phytol. 221, 233–246.
Sollins, P., Homann, P., Caldwell, B.A., 1996. Stabilization and destabilization of soil organic matter: mechanisms and controls. Geoderma 74, 65–105.
Song, X.S., Shi, S.M., Lu, S., Ren, R.X., He, C.X., Meng, P., Zhang, J.S., Yin, C.J., Zhang, X., 2021. Changes in soil chemical properties following afforestation of cropland with *Robinia pseudoacacia* in the southeastern Loess Plateau of China. Forest Ecol. Manag. 487, 118993.
Startsev, V.V., Khaydapova, D.D., Degteva, S.V., Dymov, A.A., 2020. Soils on the southern border of the cryolithozone of European part of Russia (the Subpolar Urals) and their soil organic matter fractions and rheological behavior. Geoderma 361, 114006.
Suding, K., et al., 2015. Committing to ecological restoration. Science 348, 638–640.
Sullivan, B., Nifong, R., Nasto, M.K., Alvarez-Clare, S., Dencker, C.M., et al., 2019. Biogeochemical recuperation of lowland tropical forest during succession. Ecology 10, e02641.
Sun, W.Y., Song, X.Y., Mu, X.M., Gao, P., Wang, F., Zhao, G.J., 2015. Spatiotemporal vegetation cover variations associated with climate change and ecological restoration in the Loess Plateau. Agr. Forest Meteorol. 209–210, 87–99.
Vance, E.D., Brookes, P.C., Jenkinson, D.S., 1987. An extraction method for measuring microbial biomass C. Soil Biol. Biochem. 19, 703–707.
Wander, M.M., 2004. Soil organic matter fractions and their relevance to soil function. In: Magdoff, F., Weil, R.R. (Eds.), Soil Organic Matter in Sustainable Agriculture. CRC Press, Boca Raton, FL, pp. 67–102.
Wang, M.Y., Lu, N., An, N.N., Fu, B.J., 2022. A trait-based approach for understanding changes in carbon sequestration in semi-arid grassland during succession. Ecosystems 25, 155–171.
Wang, Y.D., Xue, D.M., Hu, N., Lou, Y.L., Zhang, Q.Z., et al., 2021. Post-agricultural restoration of soil organic carbon pools across a climate gradient. Catena 200, 105138.
Williams, E.K., Fogel, M.L., Berhe, A.A., Plante, A.F., 2018. Distinct bioenergetic signatures in particulate versus mineral-associated soil organic matter. Geoderma 330, 107–116.
Wuaden, C.R., Nicoloso, R.S., Barros, E.C., Grave, R.A., 2020. Early adoption of no-till mitigates soil organic carbon and nitrogen losses due to land use change. Soil Till. Res. 204, 104728.
Xu, G.C., Cheng, S.D., Li, P., Li, Z.B., Gao, H.D., Yu, K.X., Lu, K.X., Shi, P., Cheng, Y.T., Zhao, B.H., 2018. Soil total nitrogen sources on dammed farmland under the condition of ecological construction in a small watershed on the Loess Plateau. China. Ecol. Eng. 121, 19–25.
Yan, B.S., Sun, L.P., Li, J.J., Liang, C.Q., Wei, F.R., et al., 2020. Change in composition and potential functional genes of soil bacterial and fungal communities with secondary succession in *Quercus liaotungensis* forests of the Loess Plateau, western China. Geoderma 364, 114199.
Yang, W., Zhao, H., Leng, X., Cheng, X.L., An, S.Q., 2017. Soil organic carbon and nitrogen dynamics following *Spartina alterniflora* invasion in a coastal wetland of eastern China. Catena 156, 218–289.
Yang, Y., Tilman, D., Furey, G., Lehman, C., 2019. Soil carbon sequestration accelerated by restoration of grassland biodiversity. Nat. Commun. 10, 718.
Yeasmin, S., Singh, B., Smernik, R.J., Johnston, C.T., 2020. Effect of land use on organic matter composition in density fractions of contrasting soils: a comparative study using ^{13}C NMR and DRIFT spectroscopy. Sci. Total Environ. 726, 138395.
Zhang, D., Cai, X.W., Diao, L.F., Wang, Y.Q., Wang, J.S., An, S.Q., Cheng, X.L., Yang, W., 2022. Changes in soil organic carbon and nitrogen pool sizes, dynamics, and biochemical stability during ~160 years natural vegetation restoration on the Loess Plateau, China. Catena 211, 106014.
Zhang, Z.M., Han, X.Z., Yan, J., Zou, W.X., Wang, E.T., et al., 2020. Keystone microbiomes revealed by 14 years of field restoration of the degraded agricultural soil under distinct vegetation scenarios. Front. Microbiol. 11, 1915.
Zhong, Y.Q.W., Yan, W.M., Wang, R.W., Wang, W., Shangguan, Z.P., 2018. Decreased occurrence of carbon cycle functions in microbial communities along with long-term secondary succession. Soil Biol. Biochem. 123, 207–217.
Zhong, Z.K., Wu, S.J., Lu, X.Q., Ren, Z.X., Wu, Q.M., Xu, M.P., Ren, C.J., Yang, G.H., Han, X.H., 2021. Organic carbon, nitrogen accumulation, and soil aggregate dynamics as affected by vegetation restoration patterns in the Loess Plateau of China. Catena 196, 104867.